Ab initio many-body calculations of nucleon scattering on ^{4}He, ^{7}Li, ^{7}Be, ^{12}C, and ^{16}O

Petr Navrátil,[1] Robert Roth,[2] and Sofia Quaglioni[1]
[1]*Lawrence Livermore National Laboratory, P. O. Box 808, L-414, Livermore, California 94551, USA*
[2]*Institut für Kernphysik, Technische Universität Darmstadt, D-64289 Darmstadt, Germany*
(Received 26 July 2010; revised manuscript received 3 September 2010; published 27 September 2010)

We combine a recently developed *ab initio* many-body approach capable of describing simultaneously both bound and scattering states, the *ab initio* no-core shell model/resonating-group method (NCSM/RGM), with an importance-truncation scheme for the cluster eigenstate basis and demonstrate its applicability to nuclei with mass numbers as high as 17. By using soft similarity renormalization-group-evolved chiral nucleon-nucleon interactions, we first calculate nucleon-^{4}He phase shifts, cross sections, and analyzing powers. Next, we investigate nucleon scattering on ^{7}Li, ^{7}Be, ^{12}C, and ^{16}O in coupled-channel NCSM/RGM calculations that include low-lying excited states of these nuclei. We check the convergence of phase shifts with the basis size and study $A = 8$, 13, and 17 bound and unbound states. Our calculations predict low-lying resonances in ^{8}Li and ^{8}B that have not been experimentally clearly identified yet. We are able to reproduce reasonably well the structure of the $A = 13$ low-lying states. However, we find that $A = 17$ states cannot be described without an improved treatment of ^{16}O one-particle-one-hole excitations and α clustering.

DOI: 10.1103/PhysRevC.82.034609 PACS number(s): 21.60.De, 25.10.+s, 27.10.+h, 27.20.+n

I. INTRODUCTION

Nuclei are quantum many-body systems with both bound and unbound states. A realistic *ab initio* description of light nuclei with predictive power must have the capability to describe both classes of states within a unified framework. Over the past decade, significant progress has been made in our understanding of the properties of the bound states of light nuclei starting from realistic nucleon-nucleon (NN) interactions, see, for example, Ref. [1] and references therein, and more recently also from NN plus three-nucleon (NNN) interactions [2–4]. The solution of the nuclear many-body problem becomes more complex when scattering or nuclear reactions are considered. For $A = 3$ and 4 nucleon systems, the Faddeev [5] and Faddeev-Yakubovsky [6] as well as the hyperspherical harmonics [7] or the Alt, Grassberger, and Sandhas [8] methods are applicable and successful. However, *ab initio* calculations for unbound states and scattering processes that involve more than four nucleons in total are quite challenging. The first *ab initio* many-body neutron-^{4}He scattering calculations were performed within the Green's Function Monte Carlo (GFMC) method by using the Argonne NN potential and the Illinois NNN interaction [9]. Also, resonances in He isotopes were investigated within the coupled-cluster method by using the Gamow basis [10].

In a new development, we have recently combined the *ab initio* no-core shell model (NCSM) [11] and the resonating-group method (RGM) [12–17], into a new many-body approach [18,19] (*ab initio* NCSM/RGM) capable of treating bound and scattering states of light nuclei in a unified formalism by starting from fundamental internucleon interactions. The NCSM is an *ab initio* approach to the microscopic calculation of ground and low-lying excited states of light nuclei with realistic two- and, in general, three-nucleon forces. The RGM is a microscopic cluster technique based on the use of A-nucleon Hamiltonians, with fully antisymmetric many-body wave functions built by assuming that the nucleons are grouped into clusters. Although most of its applications are based on the use of binary-cluster wave functions, the RGM can be formulated for three (and, in principle, even more) clusters in relative motion [13]. The use of the harmonic-oscillator (HO) basis in the NCSM results in an incorrect description of the wave-function asymptotic and a lack of coupling to the continuum. By combining the NCSM with the RGM, we complement the ability of the RGM to deal with scattering and reactions with the use of realistic interactions and a consistent *ab initio* description of the nucleon clusters, achieved via the NCSM. Presently, the NCSM/RGM approach has been formulated for processes that only involve binary-cluster systems. However, extensions of the approach to include three-body cluster channels are feasible also in view of recent developments on the treatment of both three-body bound and continuum states (see, e.g., Refs. [20–24]). As described in detail in Refs. [18,19], the *ab initio* NCSM/RGM approach has already been applied to study the n-^{3}H, n-^{4}He, n-^{10}Be, and p-^{3,4}He scattering processes, and to address the parity inversion of the ^{11}Be ground state by using realistic NN potentials. In those papers, we demonstrated convergence of the approach with increasing basis size in the case of the $A = 4$ and $A = 5$ scatterings. The n-^{10}Be calculations were, on the other hand, performed only in a limited basis because of the computational complexity of the NCSM calculations of the ^{10}Be eigenstates.

It is the purpose of the present paper to expand the applicability of the NCSM/RGM beyond the lightest nuclei by using sufficiently large $N\hbar\Omega$ HO excitations to guarantee convergence of the calculation with the HO-basis expansion of both the cluster wave functions and the localized RGM integration kernels. The use of large $N\hbar\Omega$ values is now feasible because of the recent introduction of the importance-truncated (IT) NCSM scheme [25,26]. It turns out that many of the basis states used in the NCSM calculations are irrelevant for the description of any particular eigenstate (e.g., the ground

state or a set of low-lying states). Therefore, if one were able to identify the important basis states beforehand, one could reduce the dimension of the matrix eigenvalue problem without losing predictive power. This can be performed by using an IT scheme based on many-body perturbation theory [25].

We make use of the IT NCSM wave functions for the cluster eigenstates, in particular, the eigenstates of the target nucleus of the binary nucleon-nucleus system and calculate the one- and two-body densities that are then used to obtain the NCSM/RGM integration kernels. We benchmark the IT approach in basis sizes accessible by the full calculation and apply it within still larger basis sizes until convergence is reached for target nuclei as heavy as ^{12}C or ^{16}O. In this paper, we employ a similarity-renormalization-group-(SRG-) [27–29] evolved chiral N^{3}LO NN potential [30] (SRG-N^{3}LO) that is soft enough to allow us reach convergence within about 14–16$\hbar\Omega$ HO excitations in the basis expansion.

In Sec. II, we briefly overview the NCSM/RGM formalism and present, for the first time, the IT-NCSM scheme that includes both ground and low-lying excited states in the set of reference states. Next, we present scattering calculation results for the n-^{4}He and p-^{4}He systems in Sec. III. In particular, we compare the calculated phase shifts to an R-matrix analysis of experimental data and, further, calculated differential cross sections and analyzing powers in the energy range 6–19 MeV to the corresponding experimental data. Neutron elastic and inelastic scatterings on ^{7}Li and proton elastic and inelastic scatterings on ^{7}Be are investigated in Sec. IV. We present phase shifts, cross sections, and scattering lengths. We predict resonances in ^{8}Li and ^{8}Be that have not been clearly identified in experiments yet. In Sec. V, we discuss nucleon-^{12}C results for both bound and unbound states of ^{13}C and ^{13}N, obtained by including two ^{12}C bound states, the ground and the first 2^+ states, in the NCSM/RGM coupled-channel calculations. In Sec. VI, we present results for the nucleon-^{16}O system. In the NCSM/RGM coupled-channel calculations, we take the ^{16}O ground state and up to the lowest three ^{16}O negative-parity states into account. Conclusions are given in Sec. VII.

II. FORMALISM

A. NCSM/RGM

The *ab inito* NCSM/RGM approach was introduced in Ref. [18] with details of the formalism given in Ref. [19]. Here, we give a brief overview of the main points.

In the present paper, we limit ourselves to a two-cluster RGM, which is based on binary-cluster channel states of total angular momentum J, parity π, and isospin T,

$$\left|\Phi^{J^\pi T}_{\nu r}\right\rangle = \left[\left(\left|A-a\alpha_1 I_1^{\pi_1} T_1\right\rangle\left|a\alpha_2 I_2^{\pi_2} T_2\right\rangle\right)^{(sT)} \times Y_\ell(\hat{r}_{A-a,a})\right]^{(J^\pi T)} \frac{\delta(r-r_{A-a,a})}{r r_{A-a,a}}. \quad (1)$$

In the preceding expression, $|A-a\alpha_1 I_1^{\pi_1} T_1\rangle$ and $|a\alpha_2 I_2^{\pi_2} T_2\rangle$ are the internal (antisymmetric) wave functions of the first and second clusters, which contain $A-a$ and a nucleons ($a < A$), respectively. They are characterized by angular momentum quantum numbers I_1 and I_2 coupled together to form channel spin s. For their parity, isospin, and additional quantum numbers, we use the notations π_i, T_i, and α_i, respectively, with $i = 1, 2$. The cluster centers of mass (c.m.s) are separated by the relative coordinate,

$$\vec{r}_{A-a,a} = r_{A-a,a}\hat{r}_{A-a,a} = \frac{1}{A-a}\sum_{i=1}^{A-a}\vec{r}_i - \frac{1}{a}\sum_{j=A-a+1}^{A}\vec{r}_j, \quad (2)$$

where $\{\vec{r}_i, i = 1, 2, \ldots, A\}$ are the A single-particle coordinates. The channel states of Eq. (1) have relative angular momentum ℓ. It is convenient to group all relevant quantum numbers into a cumulative index $\nu = \{A-a\alpha_1 I_1^{\pi_1} T_1; a\alpha_2 I_2^{\pi_2} T_2; s\ell\}$.

The former basis states can be used to expand the many-body wave function according to

$$|\Psi^{J^\pi T}\rangle = \sum_\nu \int dr\, r^2 \frac{g_\nu^{J^\pi T}(r)}{r}\hat{\mathcal{A}}_\nu\left|\Phi^{J^\pi T}_{\nu r}\right\rangle. \quad (3)$$

As the basis states, Eq. (1), are not antisymmetric under the exchange of nucleons that belong to different clusters, to preserve the Pauli principle, one has to introduce the appropriate intercluster antisymmetrizer, schematically $\hat{\mathcal{A}}_\nu = \sqrt{\frac{(A-a)!a!}{A!}}\sum_P(-)^p P$, where the sum runs over all possible permutations P that can be carried out among nucleons that pertain to different clusters, and p is the number of interchanges that characterizes them. The coefficients of the expansion Eq. (3) are the relative-motion wave functions $g_\nu^{J^\pi T}(r)$, which represent the only unknowns of the problem. To determine them, one has to solve the nonlocal integrodifferential coupled-channel equations,

$$\sum_\nu \int dr\, r^2\left[\mathcal{H}^{J^\pi T}_{\nu'\nu}(r', r) - E\mathcal{N}^{J^\pi T}_{\nu'\nu}(r', r)\right]\frac{g_\nu^{J^\pi T}(r)}{r} = 0, \quad (4)$$

where the two integration kernels, the Hamiltonian kernel,

$$\mathcal{H}^{J^\pi T}_{\nu'\nu}(r', r) = \left\langle\Phi^{J^\pi T}_{\nu' r'}\left|\hat{\mathcal{A}}_{\nu'} H \hat{\mathcal{A}}_\nu\right|\Phi^{J^\pi T}_{\nu r}\right\rangle, \quad (5)$$

and the norm kernel,

$$\mathcal{N}^{J^\pi T}_{\nu'\nu}(r', r) = \left\langle\Phi^{J^\pi T}_{\nu' r'}\left|\hat{\mathcal{A}}_{\nu'}\hat{\mathcal{A}}_\nu\right|\Phi^{J^\pi T}_{\nu r}\right\rangle, \quad (6)$$

contain all the nuclear structure and antisymmetrization properties of the problem. In particular, the nonlocality of the kernels is a direct consequence of the exchanges of nucleons between the clusters. We have used the notation E and H to denote the total energy in the c.m. frame, and the intrinsic A-nucleon microscopic Hamiltonian, respectively.

The formalism presented earlier is combined with the *ab initio* NCSM in two steps: First, we note that the Hamiltonian can be written as

$$H = T_{\rm rel}(r) + \mathcal{V}_{\rm rel} + \bar{V}_{\rm C}(r) + H_{(A-a)} + H_{(a)}, \quad (7)$$

where $H_{(A-a)}$ and $H_{(a)}$ are the $(A-a)$- and a-nucleon intrinsic Hamiltonians, respectively, $T_{\rm rel}(r)$ is the relative kinetic energy and $\mathcal{V}_{\rm rel}$ is the sum of all interactions between nucleons, which belong to different clusters after subtraction of the average Coulomb interaction between them, explicitly singled out in the term $\bar{V}_{\rm C}(r) = Z_{1\nu}Z_{2\nu}e^2/r$ ($Z_{1\nu}$ and $Z_{2\nu}$ are the

charge numbers of the clusters in channel ν). We use identical realistic potentials in both the cluster's Hamiltonians and the intercluster interaction $\mathcal{V}_{\rm rel}$. Accordingly, $|A-a\alpha_1 I_1^{\pi_1} T_1\rangle$ and $|a\alpha_2 I_2^{\pi_2} T_2\rangle$ are obtained by diagonalizing $H_{(A-a)}$ and $H_{(a)}$, respectively, in the model space spanned by the NCSM $N_{\rm max}\hbar\Omega$ HO basis. Note that, in the present paper, we use soft SRG-evolved NN potentials. Therefore, there is no need to derive any further effective interaction tailored to the model-space truncation as with these soft interactions our calculations converge in the model spaces we are able to reach.

Second, we replace the δ functions in the localized parts of the Hamiltonian Eq. (5) and the norm Eq. (6) kernels with their representation in the HO model space. We use identical HO frequency as for the cluster eigenstate wave functions and a consistent model-space size ($N_{\rm max}$). We emphasize that this replacement is only performed for the localized parts of the kernels. The diagonal parts that come from the identity operator in the antisymmetrizers, the kinetic term, and the average Coulomb potential are treated exactly.

In this paper, we apply the NCSM/RGM formalism in the single-nucleon projectile basis [i.e., for binary-cluster channel states Eq. (1) with $a=1$ (with channel index $\nu = \{A-1\alpha_1 I_1^{\pi_1} T_1; 1\frac{1}{2}\frac{1}{2}; s\ell\})$]. As an illustration, let us discuss the norm kernel that is rather simple in this basis in more detail:

$$\mathcal{N}^{J^\pi T}_{\nu'\nu}(r',r) = \left\langle \Phi^{J^\pi T}_{\nu' r'} \middle| 1 - \sum_{i=1}^{A-1} \hat{P}_{iA} \middle| \Phi^{J^\pi T}_{\nu r} \right\rangle \tag{8}$$

$$= \delta_{\nu'\nu}\frac{\delta(r'-r)}{r'r} - (A-1)\sum_{n'n} R_{n'\ell'}(r')R_{n\ell}(r) \times \left\langle \Phi^{J^\pi T}_{\nu' n'} \middle| \hat{P}_{A-1,A} \middle| \Phi^{J^\pi T}_{\nu n} \right\rangle. \tag{9}$$

We can easily recognize a direct term in which the initial and final states are identical [corresponding to diagram (a) of Fig. 1], and a many-body correction due to the exchange part of the intercluster antisymmetrizer [corresponding to diagram (b) of Fig. 1]. We note that, in calculating the matrix elements of the exchange operator $\hat{P}_{A-1,A}$, we replaced the δ function of Eq. (1) with its representation in the HO model space as previously discussed. This is appropriate as the transposition $\hat{P}_{A-1,A}$ operator, which acts on the target wave function in the short-to-medium range. On the contrary, the δ function, which comes from the identity, is treated exactly. The presence of the intercluster antisymmetrizer also affects the Hamiltonian kernel, and, in particular, the matrix elements of the interaction. For an NN potential, one obtains a direct term, which involves the interaction and exchange of two nucleons only [see diagrams (c) and (d) of Fig. 1], and an exchange term, which involves three nucleons. Diagram (e) of Fig. 1 describes this latter term in which the last nucleon is exchanged with one of the nucleons of the first cluster and interacts with yet another nucleon. For more details on the integration kernels in the single-nucleon projectile basis, we refer the readers to Ref. [19].

By being translationally invariant quantities, the norm and Hamiltonian kernels can be naturally derived by working within the NCSM Jacobi-coordinate basis. However, by

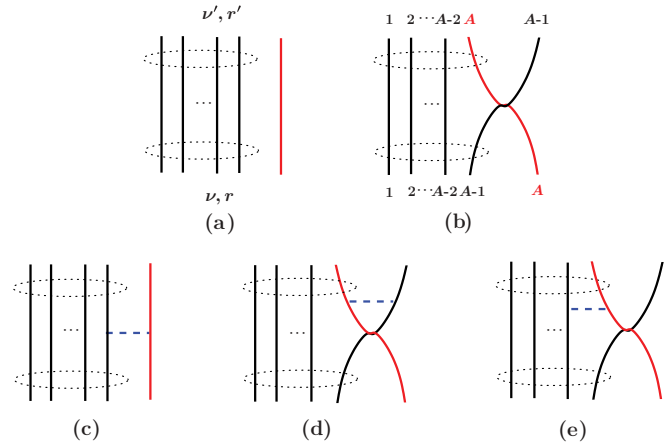

FIG. 1. (Color online) Diagrammatic representation of: (a) direct and (b) exchange components of the norm kernel; (c) and (d) direct and (e) exchange components of the potential kernel. The group of circled black lines represents the target cluster, a state of $A-1$ nucleons. The separate red line represents the projectile, a single nucleon. Bottom and upper parts of the diagram represent initial and final states, respectively.

introducing Slater-determinant (SD) channel states of the type,

$$\left|\Phi^{J^\pi T}_{\nu n}\right\rangle_{\rm SD} = \left[\left(|A-a\alpha_1 I_1 T_1\rangle_{\rm SD}|a\alpha_2 I_2 T_2\rangle\right)^{(sT)} \times Y_\ell\left(\hat{R}^{(a)}_{\rm c.m.}\right)\right]^{(J^\pi T)} R_{n\ell}\left(R^{(a)}_{\rm c.m.}\right), \tag{10}$$

in which the eigenstates of the $(A-a)$-nucleon fragment are obtained in the SD basis (while the second cluster is still an NCSM Jacobi-coordinate eigenstate), it can easily be demonstrated that translationally invariant matrix elements can be extracted from those calculated in the SD basis of Eq. (10) by inverting the following expression:

$$\begin{aligned}{}_{\rm SD}\left\langle \Phi^{J^\pi T}_{\nu' n'} \middle| \hat{\mathcal{O}}_{\rm t.i.} \middle| \Phi^{J^\pi T}_{\nu n} \right\rangle_{\rm SD} &= \sum_{n'_r\ell'_r, n_r\ell_r, J_r} \left\langle \Phi^{J^{\pi_r} T}_{\nu'_r n'_r} \middle| \hat{\mathcal{O}}_{\rm t.i.} \middle| \Phi^{J^{\pi_r} T}_{\nu_r n_r} \right\rangle \\ &\times \sum_{NL} \hat{\ell}\hat{\ell}'\hat{J}_r^2 (-1)^{(s+\ell-s'-\ell')} \begin{Bmatrix} s & \ell_r & J_r \\ L & J & \ell \end{Bmatrix} \begin{Bmatrix} s' & \ell'_r & J_r \\ L & J & \ell' \end{Bmatrix} \\ &\times \langle n_r\ell_r NL\ell|00n\ell\ell\rangle_{a/(A-a)} \langle n'_r\ell'_r NL\ell|00n'\ell'\ell'\rangle_{a/(A-a)}. \end{aligned} \tag{11}$$

Here, $\hat{\mathcal{O}}_{\rm t.i.}$ represents any scalar and parity-conserving translational-invariant operator ($\hat{\mathcal{O}}_{\rm t.i.} = \hat{\mathcal{A}}$, $\hat{\mathcal{A}}H\hat{\mathcal{A}}$, etc.) and $\langle n_r\ell_r NL\ell|00n\ell\ell\rangle_{a/(A-a)}$ are generalized HO brackets for two particles with the mass ratio $a/(A-a)$. We exploited both Jacobi-coordinate and SD channel states to verify our results. The use of the SD basis is computationally advantageous and allows us to explore reactions that involve p-shell nuclei, as done in the present paper. To calculate the parts of the integration kernels depicted in Figs. 1(b)–1(d), all information that we need from the SD-basis calculation are one-body densities of the target eigenstates. For the (e) part of the integration kernel in Fig. 1, we need two-body densities of the target eigenstates obtained in the SD basis.

Because of the presence of the norm kernel $\mathcal{N}_{\nu'\nu}^{J^\pi T}(r', r)$, Eq. (4) does not represent a system of multichannel Schrödinger equations, and $g_\nu^{J^\pi T}(r)$ do not represent Schrödinger wave functions. The short-range nonorthogonality, induced by the nonidentical permutations in the intercluster antisymmetrizers, can be removed by introducing normalized Schrödinger wave functions,

$$\frac{\chi_\nu^{J^\pi T}(r)}{r} = \sum_\gamma \int dy\, y^2 \mathcal{N}_{\nu\gamma}^{1/2}(r, y) \frac{g_\gamma^{J^\pi T}(y)}{y}, \tag{12}$$

where $\mathcal{N}^{1/2}$ is the square root of the norm kernel and by applying the inverse-square root of the norm kernel $\mathcal{N}^{-1/2}$ to both left- and right-hand sides of the square brackets in Eq. (4). This procedure, explained in more detail in Ref. [19], leads to a system of multichannel Schrödinger equations,

$$\left[\hat{T}_{\rm rel}(r) + \bar{V}_{\rm C}(r) - \left(E - E_{\alpha_1}^{I_1^{\pi_1} T_1} - E_{\alpha_2}^{I_2^{\pi_2} T_2}\right)\right] \frac{\chi_\nu^{J^\pi T}(r)}{r} + \sum_{\nu'} \int dr'\, r'^2 W_{\nu\nu'}^{J^\pi T}(r, r') \frac{\chi_{\nu'}^{J^\pi T}(r')}{r'} = 0, \tag{13}$$

where $E_{\alpha_i}^{I_i^{\pi_i} T_i}$ is the energy eigenvalue of the ith cluster ($i = 1, 2$), and $W_{\nu'\nu}^{J^\pi T}(r', r)$ is the overall nonlocal potential between the two clusters, which depends on the channel of relative motion, while it does not depend on the energy. These are the equations that we finally solve to obtain both our scattering and our bound-state results.

B. IT-NCSM with excited states

The primary limitation for the range of applicability of the NCSM in terms of particle number A and model-spaces size $N_{\rm max}$ results from the factorial growth of the dimension of the $N_{\rm max}\hbar\Omega$ space. Except for light isotopes, it is hardly possible to obtain a converged result by using a bare Hamiltonian within the $N_{\rm max}\hbar\Omega$ spaces that are computationally tractable.

At this point, the IT offers a solution. The IT in connection with the NCSM was introduced in Ref. [25] and was discussed in detail in Ref. [26]. In the following, we summarize a few key features of the IT-NCSM and generalize the approach to the simultaneous description of excited states.

The motivation for the IT results from the observation that the expansion of any particular eigenstate of the Hamiltonian in a full m-scheme NCSM space typically contains a large number of basis states with extremely small or vanishing amplitudes. The amplitudes define an adaptive truncation criterion, which takes the properties of the Hamiltonian and the structure of the eigenstate under consideration into account. If those amplitudes were known—at least approximately—before actually solving the eigenvalue problem, one could reduce the model space to the most relevant basis states by imposing a threshold on the amplitude. The amplitude of a particular basis state $|\Phi_\nu\rangle$ in the expansion of a specific eigenstate can be estimated by using first-order multiconfigurational perturbation theory. To set up a perturbation series, we need an initial approximation of the target state, the so-called reference state $|\Psi_{\rm ref}\rangle$. In practice, this reference state will be a superposition of basis states $|\Phi_\mu\rangle \in \mathcal{M}_{\rm ref}$ from a reference space $\mathcal{M}_{\rm ref}$:

$$|\Psi_{\rm ref}\rangle = \sum_{\mu\in\mathcal{M}_{\rm ref}} C_\mu^{\rm (ref)} |\Phi_\mu\rangle. \tag{14}$$

The reference state and the amplitudes $C_\mu^{\rm (ref)}$ are typically extracted from a previous NCSM calculation. Based on $|\Psi_{\rm ref}\rangle$ as the unperturbed state, we can evaluate the first-order perturbative correction to the target state, which results from basis states $|\Phi_\nu\rangle \notin \mathcal{M}_{\rm ref}$. Their first-order amplitude defines the so-called importance measure,

$$\kappa_\nu = -\frac{\langle\Phi_\nu|H|\Psi_{\rm ref}\rangle}{\epsilon_\nu - \epsilon_{\rm ref}} = -\sum_{\mu\in\mathcal{M}_{\rm ref}} C_\mu^{\rm (ref)} \frac{\langle\Phi_\nu|H|\Phi_\mu\rangle}{\epsilon_\nu - \epsilon_{\rm ref}}. \tag{15}$$

The energy denominator $\epsilon_\nu - \epsilon_{\rm ref}$ in a Møller-Plesset-type partitioning is simply given by the unperturbed HO excitation energy of the basis state $|\Phi_\nu\rangle$ (see Ref. [26] for details).

By imposing an importance threshold $\kappa_{\rm min}$, we construct an IT model space by including all basis states with importance measure $|\kappa_\nu| \geqslant \kappa_{\rm min}$. Since the importance measure is zero for all basis states that differ from all of the states in $\mathcal{M}_{\rm ref}$ by more than a two-particle-two-hole excitation, we have to embed the construction of the IT space into an iterative update cycle. After constructing the IT space and solving the eigenvalue problem in that space, we obtain an improved approximation for the target state that defines a reference state for the next iteration. To accelerate the evaluation of the importance measure Eq. (15), we typically do not use the complete eigenstate as the new reference state, but project it onto a reference space spanned by the basis states with $|C_\nu| \geqslant C_{\rm min}$, where C_ν are the coefficients that result from the solution of the eigenvalue problem. The second threshold $C_{\rm min}$ will be chosen sufficiently small so as not to affect the results for a given $\kappa_{\rm min}$ threshold.

Simple iterative update schemes can be devised for any type of full model spaces, as discussed in Refs. [26,31]. Specifically for the $N_{\rm max}\hbar\Omega$ space of the NCSM, however, there is an efficient sequential update scheme, which leads to the IT-NCSM(seq) approach. It is based on the fact that all states of an $(N_{\rm max} + 2)\hbar\Omega$ space can be generated from the basis states of an $N_{\rm max}\hbar\Omega$ space by using two-particle-two-hole excitations at most. Thus, a single importance update, which starts from a reference state in an $N_{\rm max}\hbar\Omega$ space gives access to all relevant states in an $(N_{\rm max} + 2)\hbar\Omega$ space. By making use of this property, in the IT-NCSM(seq) we start with a full NCSM calculation in, for example, $2\hbar\Omega$ and use this eigenstate after applying the $C_{\rm min}$ threshold as a reference state for constructing the IT $4\hbar\Omega$ space. After solving the eigenvalue problem for this IT $4\hbar\Omega$ space, we use the resulting eigenstate as a reference state to construct the $6\hbar\Omega$ space, and so on. Thus, only one importance update is required for each value of $N_{\rm max}$, which makes this scheme very efficient computationally. Moreover, in the limit of vanishing thresholds, $(\kappa_{\rm min}, C_{\rm min}) \to 0$, this scheme recovers the full $N_{\rm max}\hbar\Omega$ space at each step of the sequence [i.e., the IT-NCSM(seq) would recover the full NCSM result].

Based on this limiting property, we can obtain a numerical approximation for the full NCSM result by extrapolating the

IT-NCSM(seq) observables obtained for a set of different importance thresholds $\kappa_{\min}$ (and, in principle, also $C_{\min}$) to $\kappa_{\min} \to 0$. Through this extrapolation, the contribution of discarded basis states (i.e., those with importance measures $|\kappa_\nu|$ below the smallest threshold considered) is effectively recovered. Because the control parameter $\kappa_{\min}$ is tied to the physical structure of the eigenstate, we observe a smooth threshold dependence for all observables, which allows for a robust threshold extrapolation. In the case of the energy, we can improve the quality of the extrapolation further by considering a perturbative second-order estimate for the energy of the excluded basis states. While setting up the IT space, all second-order energy contributions,

$$\xi_\nu = -\frac{|\langle \Phi_\nu | H | \Psi_{\rm ref} \rangle|^2}{\epsilon_\nu - \epsilon_{\rm ref}} \tag{16}$$

for the discarded states with $|\kappa_\nu| < \kappa_{\min}$ are summed up to provide a correction $\Delta_{\rm excl}(\kappa_{\min})$ to the energy eigenvalue. By construction, this correction goes to zero in the limit $\kappa_{\min} \to 0$. We use this additional information for a constrained simultaneous extrapolation of the energy-to-vanishing threshold with and without perturbative correction for the excluded states as described in detail in Ref. [26].

The whole concept can be generalized for the description of excited states. For the present application in connection with the NCSM/RGM, we aim at an IT model space that is equally well suited for the description of the lowest M eigenstates of the Hamiltonian for given parity and total angular momentum projection. Instead of using a single reference state, we employ different reference states $|\Psi_{\rm ref}^{(m)}\rangle$, with $m = 1, \ldots, M$, for each of the M target states. For each reference state, we define a separate importance measure $\kappa_\nu^{(m)}$ following Eq. (15). A basis state $|\Phi_\nu\rangle$ is included in the IT space if at least one of the importance measures $|\kappa_\nu^{(m)}|$ is above the threshold $\kappa_{\min}$ (i.e., if it is relevant for the description of at least one of the M target states, it will be included). Because the different eigenstates are typically dominated by different basis states, the dimension of the IT space grows linearly with M.

In the IT-NCSM(seq) scheme, we start with a full NCSM calculation in $2\hbar\Omega$ and use the lowest M eigenstates as initial reference states $|\Psi_{\rm ref}^{(m)}\rangle$. Based on the corresponding importance measures $\kappa_\nu^{(m)}$, the IT $4\hbar\Omega$ space is constructed, and the lowest M eigenvectors in this space serve as new reference states (after application of the $C_{\min}$ threshold) for the construction of the $6\hbar\Omega$ space, and so on. From a sequence of IT-NCSM(seq) calculations, we obtain a set of M eigenvectors for each value of $N_{\max}$, which can be used to evaluate other observables.

By default, we compute the expectation values of $\vec{J}^2$ and $\vec{T}^2$ as well as the expectation values of $H_{\rm int}$ and $H_{\rm c.m.}$. Indeed, since we use an IT space in the m scheme without explicit angular momentum projection, the eigenstates are not guaranteed to have good angular momentum and isospin. Therefore, we monitor the expectation values of $\vec{J}^2$ and $\vec{T}^2$ and find values, which typically differ by less than 10^{-3} from the exact quantum numbers. As in the full NCSM, we separate spurious c.m. excitations from the physical spectrum by adding a Lawson term $\beta H_{\rm c.m.}$ to the translationally invariant intrinsic Hamiltonian $H_{\rm int}$ (with the typical choice $\beta = 10$). At the same time, the use of this modified Hamiltonian provides a diagnostic for potential c.m. contaminations of the intrinsic states induced by the IT. As discussed in Refs. [26,32], the independence of the intrinsic energies $\langle H_{\rm int}\rangle$ on β and the smallness of $\langle H_{\rm c.m.}\rangle$ demonstrate that the IT-NCSM(seq) solutions are free of c.m. contaminations.

Eventually, the wave functions obtained in the IT-NCSM(seq) together with the threshold extrapolated intrinsic energies form the input for the NCSM/RGM calculations discussed in the following.

III. NUCLEON-^{4}He SCATTERING

The purpose of the nucleon-^{4}He calculations presented in this paper is twofold. First, we want to check the predictive power of the SRG-evolved chiral interaction in the $A = 5$ system, where a lot of experimental scattering data exist and where our calculations can easily be converged with respect to the size of the basis expansion. Second, we want to benchmark the IT scheme with the full-space calculations all the way up to very large $N_{\max}\hbar\Omega$ spaces.

The first *ab initio* $A = 5$ scattering calculations were reported in Ref. [9]. The n-α low-lying $J^\pi = 3/2^-$ and $1/2^-$ P-wave resonances as well as the $1/2^+$ S-wave nonresonant scattering below 5-MeV c.m. energy were obtained by using the AV18 NN potential with and without the three-nucleon force, chosen to be either the Urbana IX or the Illinois-2 model. The results of these GFMC calculations revealed sensitivity to the internucleon interaction, and, in particular, to the strength of the spin-orbit force.

Soon after, the development of the *ab initio* NCSM/RGM approach allowed us to calculate both n- and (for the first time) p-α scattering phase shifts for energies up to the inelastic threshold [18,19], by using several realistic NN potentials, which include the chiral N^{3}LO [30], the $V_{\text{low}\,k}$ [33], and the charge-dependent (CD)-Bonn [34] NN potentials. Nucleon-α scattering provides one of the best-case scenarios for the application of the NCSM/RGM approach. This process is characterized by a single open channel up to the $d + {}^3$H threshold, which is fairly high in energy. In addition, the low-lying resonances of the ^{4}He nucleus are narrow enough to be reasonably reproduced by diagonalizing the four-body Hamiltonian in the NCSM model space. In the present paper, we include the first excited state of ^{4}He, the 0^+0 state, as a closed channel in our NCSM/RGM basis space.

A. Convergence with the size of the HO-basis expansion

We performed extensive nucleon-^{4}He calculations with the SRG-N^{3}LO NN potential with $\Lambda = 2.02$ fm^{-1} to check convergence of our NCSM/RGM calculations. In Fig. 2, we present n-^{4}He phase-shift results for the S and P waves obtained by using an HO-basis expansion up to $N_{\max} = 17$ for for the localized parts of the NCSM/RGM integration kernels and for the ^{4}He ground and the first excited 0^+0 wave functions (since these states have positive parity, the $N_{\max} - 1$ expansion is, in fact, used for the ^{4}He eigenstates). As seen in the figure, the phase-shift convergence is excellent.

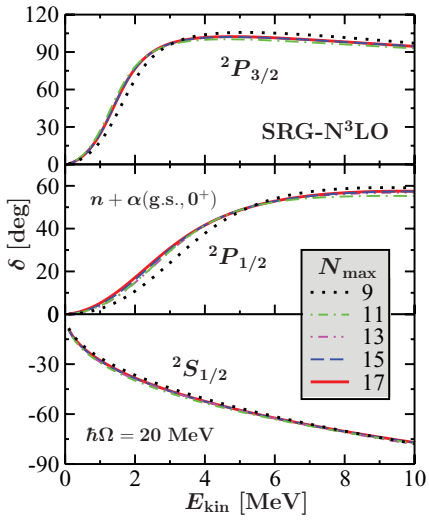

FIG. 2. (Color online) Dependence of the n-^{4}He phase shifts on the size of the HO-basis expansion of the ^{4}He wave functions and the localized parts of the integration kernels. The ^{4}He ground state and the first 0^+0 excited states were included. The SRG-N^{3}LO NN potential with $\Lambda = 2.02$ fm^{-1} and the HO frequency $\hbar\Omega = 20$ MeV were used.

In particular, the $N_{\max} = 17$ and the $N_{\max} = 15$ curves lie on top of each other. The convergence rate demonstrated here is quite similar to that obtained by using the $V_{\text{low}\,k}$ NN potential in our earlier study (compare the present Fig. 2 to the left panel of Fig. 13 in Ref. [19]).

B. Benchmark of IT calculations

As shown in Sec. III A, for the $A = 5$ system, we are able to reach complete convergence with ^{4}He wave functions obtained within full nontruncated NCSM calculations. We can, therefore, test the performance of the IT-NCSM scheme in this system all the way up to very large $N_{\max}$ values and see how well the IT-NCSM scheme reproduces the completely converged results. It should be noted that for heavier $A = 8$, 13 and $A = 17$ systems investigated later, full nontruncated NCSM calculations for the $A = 7$ ($A = 12$, 16) target nuclei are feasible only up to $N_{\max} = 10$ ($N_{\max} = 8$). It is, therefore, desirable and important to benchmark the IT-NCSM calculations in a lighter system, such as $A = 5$ in $N_{\max} > 10$ calculations.

In Fig. 3, we compare n-^{4}He phase shifts calculated within the NCSM/RGM with ^{4}He wave functions obtained in a full $N_{\max} = 16$ NCSM calculation and those obtained by using ^{4}He wave functions obtained within an $N_{\max} = 16$ IT-NCSM calculation. The agreement of the two sets of phase shifts is excellent. It should be noted that the dimension of the full $N_{\max} = 16$ ^{4}He NCSM basis is 6 344 119. The dimension of the IT-NCSM basis used here to calculate the ^{4}He wave functions was just 992 578, more than a factor of 6 smaller. Truncation parameters $\kappa_{\min} = 10^{-5}$ and $C_{\min} = 2 \times 10^{-4}$ were used. The ground-state energy from the full NCSM calculation is -28.224 MeV. The $\kappa_{\min} \to 0$ extrapolated ground-state energy from the IT-NCSM calculation is $-28.217(5)$ MeV with a difference from the full result less than 10 keV. The

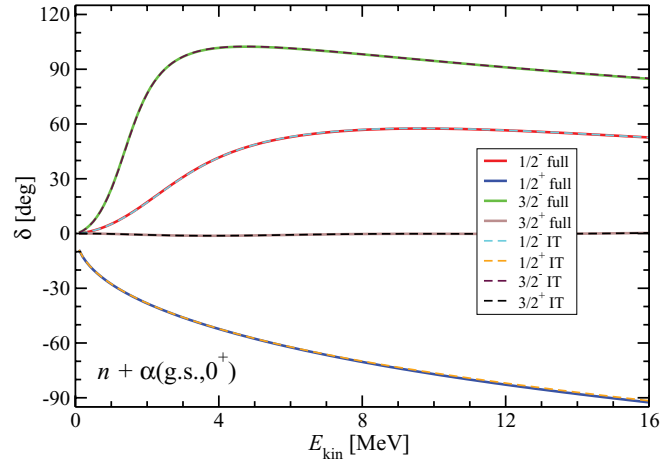

FIG. 3. (Color online) Calculated n-^{4}He S- and P-wave phase shifts. Results obtained with ^{4}He wave functions from full NCSM (solid lines) and IT-NCSM (dashed lines) calculations are compared. The SRG-N^{3}LO NN potential with $\Lambda = 2.02$ fm^{-1}, the $N_{\max} = 17$ basis space, and the HO frequency $\hbar\Omega = 20$ MeV were used. See text for details on the IT-NCSM calculation.

0^+0 excitation energy obtained in the full NCSM calculation was 21.58 MeV. The corresponding extrapolated IT-NCSM result was 21.4(1) MeV. The slightly lower accuracy of the excited-state reproduction in the IT-NCSM calculation is manifested in a very small deviation of the S-wave phase shift at energies above 12 MeV (less than 1° at 16 MeV). It should be noted that the excited 0^+0 state is not bound for small $N_{\max}$. Consequently, it is challenging to reproduce the excited state as well as the ground state in a sequential IT calculation. It should also be pointed out that unlike for the energies, no phase-shift extrapolation was performed. The needed one- and two-body densities were calculated from the wave functions obtained in the IT-NCSM calculation with the truncation parameters described previously. The excellent agreement of the full and the IT-NCSM phase shifts demonstrates that no extrapolation was actually necessary. Obviously, we can check the dependence of observables, such as phase shifts on the $\kappa_{\min}$ and $C_{\min}$ and can perform an extrapolation for vanishing values of these parameters if needed.

C. Comparison with experimental data

Our calculated n-^{4}He and p-^{4}He phase shifts are compared to those obtained from an R-matrix analysis of N-^{4}He experimental data [35] in Fig. 4. The agreement is quite reasonable for the S wave, D wave, and $^2P_{1/2}$ wave. The $^2P_{3/2}$ resonance is positioned at higher energy in the calculation, and the corresponding phase shifts are underestimated with respect to the R-matrix results, although the disagreement becomes less and less pronounced starting at about 8 MeV. While the inclusion of negative-parity excited states of the α particle would likely increase the $^2P_{3/2}$ phase shifts [18,19] somewhat, the observed difference is largely caused by a reduction in spin-orbit strength caused by the neglect of the three-nucleon interaction in our calculations. The importance of the three-nucleon force in reproducing the R matrix $^2P_{3/2}$ phase shifts was demonstrated in the GFMC n-^{4}He calculations of Ref. [9].

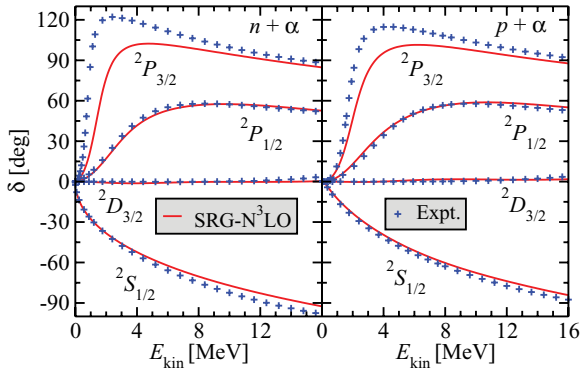

FIG. 4. (Color online) Calculated n-^{4}He (left panels) and p-^{4}He (right panels) compared to the R-matrix analysis of experimental data [35]. The NCSM/RGM calculations that included the ^{4}He ground state and the 0^+0 excited state were performed by using the SRG-N^{3}LO NN potential with $\Lambda = 2.02$ fm^{-1}. The HO frequency $\hbar\Omega =$ 20 MeV and $N_{max} = 17$ basis space were employed.

Overall, the present results obtained with the SRG-N^{3}LO NN interaction agree better with the experiment than our earlier calculations [18,19] with the $V_{low\,k}$, N^{3}LO, and CD-Bonn NN potentials. The only exception is the S-wave phase shift, which is best described by using the CD-Bonn NN potential. The larger spin-orbit strength of the employed SRG-N^{3}LO potential with respect to N^{3}LO itself is likely responsible for the improved agreement.

As our calculated phase shifts agree with the experimental ones reasonably well above the c.m. energy of 8 MeV, we expect a similar behavior for cross section and analyzing power in that energy range. This is indeed the case as shown in Fig. 5, where the calculated differential cross section and analyzing power are compared to experimental data from Karlsruhe [36] with polarized neutrons of $E_n = 17$-MeV laboratory energy. For the cross-sectional experimental data, see also references in Ref. [36]. The cross section is reproduced remarkably well at all angles, and the analyzing power is in reasonable agreement with the data, particularly at backward angles. The same quality of agreement can be found for all energies far from the low-lying resonances, as shown in the right panel of Fig. 5 for the analyzing power at $E_n = 15$ and 19 MeV.

A better display of the dependence of our calculated cross section and analyzing power upon the incident nucleon energy is provided by Fig. 6, where the p-^{4}He results for these observables are compared to the data of Ref. [37] at the proton laboratory energies of $E_p = 5.95$, 7.89, 9.89, and 11.99 MeV. As expected from the behavior of the phase shifts described earlier, for energies relatively close to the resonance region, we find a rather poor agreement with the experiment, particularly noticeable in the analyzing power overall and in the cross section at backward angles. However, starting at about 10 MeV, the agreement improves substantially, and data are once again reproduced in a quite satisfactory way at higher energies, as shown in Fig. 7, where the NCSM/RGM p-^{4}He results are compared to various experimental data sets [37–40] in the energy range $E_p \sim$ 12–17 MeV.

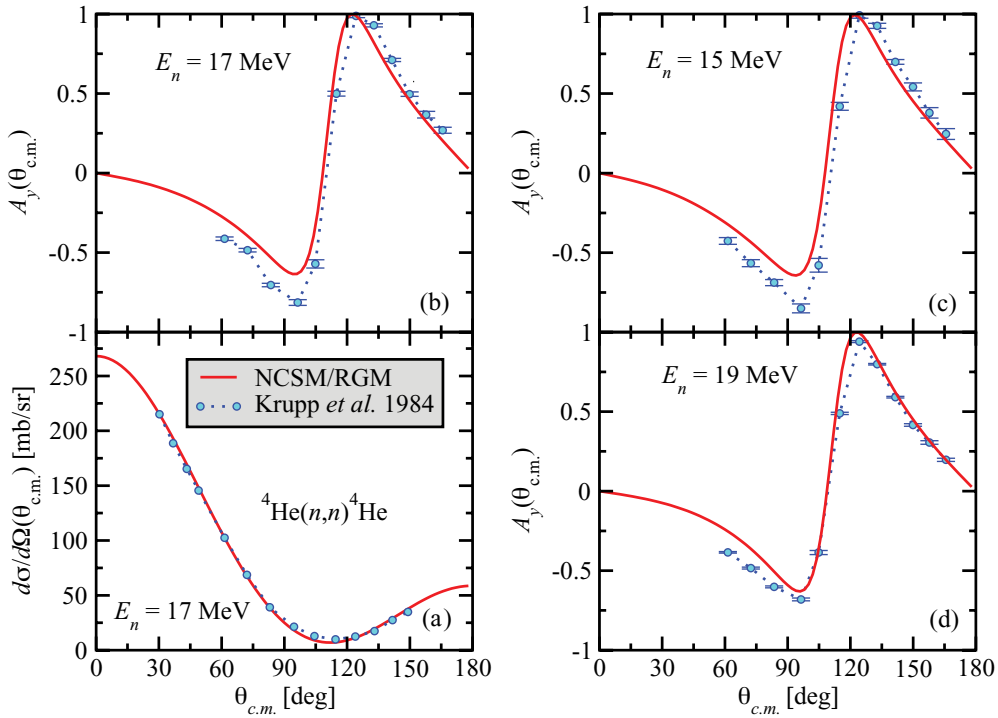

FIG. 5. (Color online) Calculated n-^{4}He differential cross section for neutron laboratory energy of (a) $E_n = 17$ MeV, and analyzing power for (b) $E_n = 17$, (c) 15, and (d) 19 MeV compared to experimental data from Ref. [36]. The NCSM/RGM results include the ^{4}He ground state and the first 0^+0 excited state and were obtained by using the SRG-N^{3}LO NN potential with $\Lambda = 2.02$ fm^{-1} for an HO frequency $\hbar\Omega = 20$ MeV and basis space size $N_{max} = 17$.

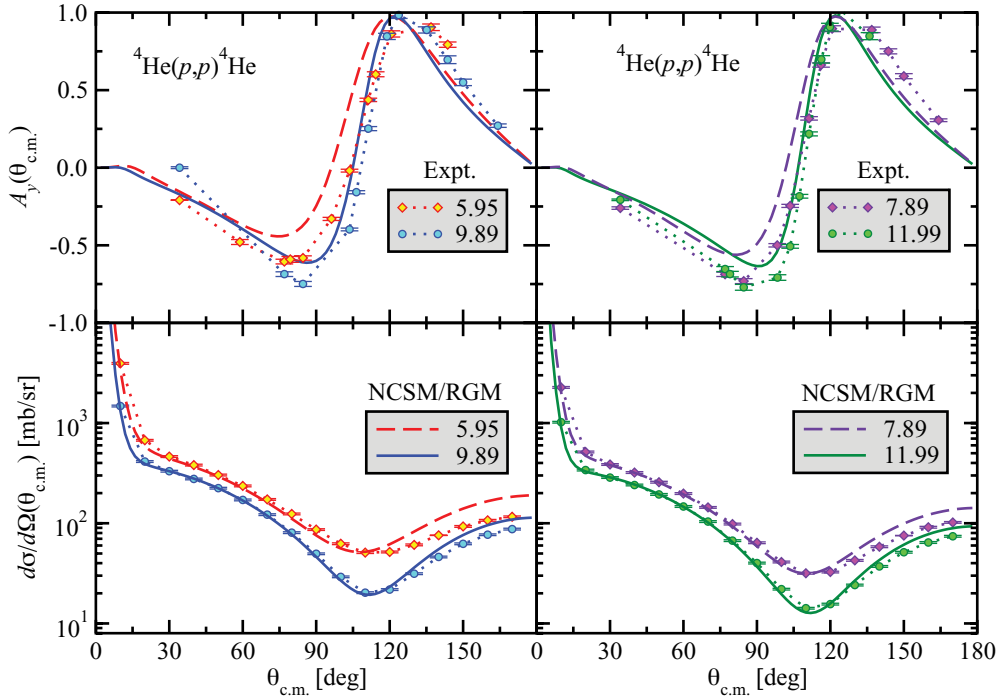

FIG. 6. (Color online) Calculated p-^{4}He differential cross section (bottom panels) and analyzing power (top panels) for proton laboratory energies of $E_p = 5.95$, 7.89, 9.89, and 11.99 MeV compared to experimental data from Ref. [37]. The NCSM/RGM results include the ^{4}He ground state and the first 0^+0 excited state and were obtained by using the SRG-N^{3}LO NN potential with $\Lambda = 2.02$ fm^{-1} for an HO frequency $\hbar\Omega = 20$ MeV and basis space size $N_{\max} = 17$.

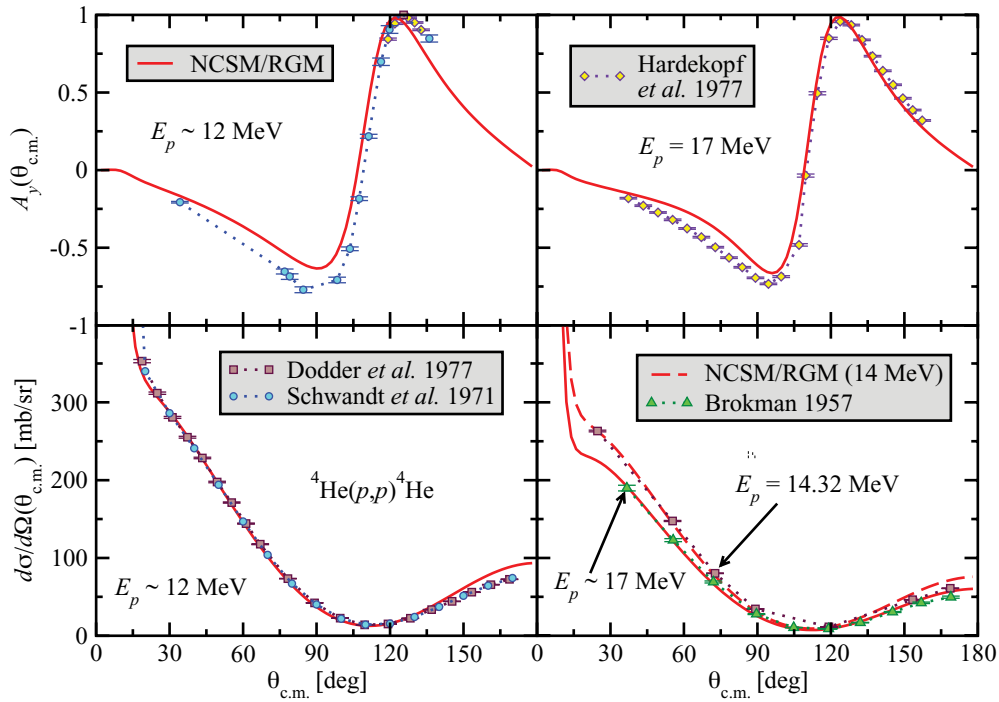

FIG. 7. (Color online) Calculated p-^{4}He differential cross section (bottom panels) and analyzing power (top panels) for proton laboratory energies $E_p = 12$, 14.32, and 17 MeV compared to experimental data from Schwandt *et al.* [37], Brokman [38], Dodder *et al.* [39], and Hardekopf and Holsen [40]. The NCSM/RGM results include the ^{4}He ground state and the first 0^+0 excited state and were obtained by using the SRG-N^{3}LO NN potential with $\Lambda = 2.02$ fm^{-1} for an HO frequency $\hbar\Omega = 20$ MeV and basis space size $N_{\max} = 17$.

TABLE I. Calculated ground-state energies of ^{3}H, ^{4}He, ^{7}Li, and ^{7}Be obtained by using the SRG-N^{3}LO NN potential with $\Lambda = 2.02$ fm^{-1} compared to experimental values.

$E_{\text{g.s.}}$ (MeV)	^{3}H	^{4}He	^{7}Li	^{7}Be
Calc.	−8.32	−28.22	−39.4(2)	−37.8(2)
Expt.	−8.48	−28.30	−39.24	−37.60

IV. NEUTRON-^{7}Li AND PROTON-^{7}Be SCATTERING

The ^{7}Be$(p,\gamma)^8$B capture reaction plays a very important role in nuclear astrophysics as it serves as an input for understanding the solar neutrino flux [41]. While the experimental determination of the neutrino flux from ^{8}B has an accuracy of about 9% [42], the theoretical predictions have uncertainties on the order of 20% [43,44]. The theoretical neutrino flux depends on the ^{7}Be$(p,\gamma)^8$B S factor. Significant experimental and theoretical effort has been devoted to studying this reaction. The S-factor extrapolation to astrophysically relevant energies depends, among other things, on the scattering lengths of the proton scattering on ^{7}Be. Experimental determination of these lengths was performed recently [45] with precision on the order of 30%. The proton-^{7}Be elastic scattering was also investigated in Ref. [46]. To benchmark the theoretical calculations used for S-factor extrapolations, an investigation of the mirror capture reaction ^{7}Li$(n,\gamma)^8$Li, as well as the $n + ^7$Li scattering is important. For example, the $n + ^7$Li scattering lengths are known with a higher accuracy [47].

The first applications of the NCSM approach to the description of the ^{7}Be$(p,\gamma)^8$B capture reaction [48] required a phenomenological correction of the asymptotic behavior of the overlap functions and, further, the scattering $p + ^7$Be wave function was calculated from a phenomenological potential model. The present investigation within the *ab initio* NCSM/RGM approach paves the way for a complete first-principles calculation of this capture reaction. Here, we limit ourselves to scattering calculations and postpone the capture reaction calculations to a forthcoming paper.

Our current limit on the unrestricted NCSM calculations for ^{7}Li and ^{7}Be is $N_{\max} = 10$. To improve the convergence of our scattering calculations, we utilize wave functions obtained within the IT-NCSM. In that scheme, we are able to reach $N_{\max} = 18$ model spaces and calculate both ground as well as low-lying excited states. This is demonstrated in Fig. 8. With the SRG-N^{3}LO NN potential with $\Lambda = 2.02$ fm^{-1} employed in the present paper, we already reach convergence around $N_{\max} = 12$–14. Also, as seen in the figure, the agreement between the unrestricted NCSM and the IT-NCSM is perfect up to the highest accessible unrestricted space $N_{\max} = 10$. Our calculated ground-state energies of ^{3}H, ^{4}He, ^{7}Li, and ^{7}Be obtained with the SRG-N^{3}LO NN potential with $\Lambda = 2.02$ fm^{-1} are summarized in Table I.

A. n-^{7}Li

The NCSM/RGM coupled-channel calculations performed for the $A = 8$ system include the ^{7}Li (^{7}Be) ground state,

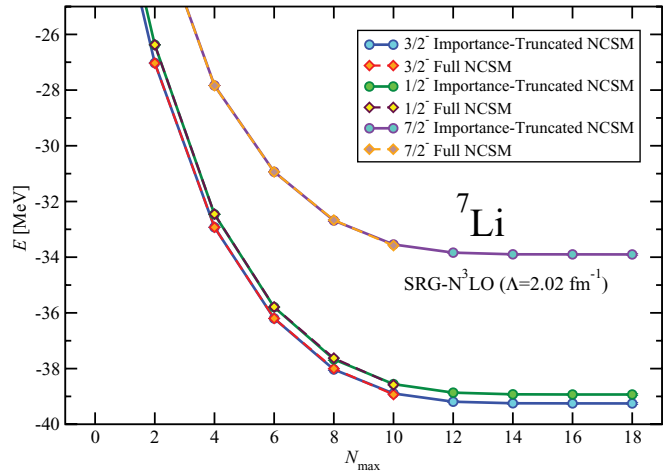

FIG. 8. (Color online) ^{7}Li ground-state and the $1/2^-$ and $7/2^-$ excited-state energy dependences on the model-space size $N_{\max}$, obtained within the IT-NCSM (solid lines), by using the SRG-N^{3}LO NN potential with $\Lambda = 2.02$ fm^{-1}. The HO frequency $\hbar\Omega = 20$ MeV was employed. The full-space NCSM results are shown by dashed lines.

the first excited $1/2^-$ state as well as the second excited $7/2^-$ state. It is essential to include the $7/2^-$ state to reproduce the low-lying 3^+ resonance in ^{8}Li and ^{8}B. By using these three states, we are able to reach model spaces up to $N_{\max} = 12$, which is sufficient concerning the HO-basis expansion convergence as can be judged from Fig. 8. The coupled-channel calculation described previously gives two bound states for the n-^{7}Li system, a 2^+, which corresponds to the experimentally observed ^{8}Li ground state, bound by 2.03 MeV [49], and a 1^+, which corresponds to the ^{8}Li first excited state at $E_x = 0.98$ MeV, bound by 1.05 MeV [49]. The calculated states are bound by 1.16 and 0.17 MeV, respectively (i.e., less than in the experiment). This is, in part, because of the fact that higher excited states of ^{7}Li were omitted. In Fig. 9, we present our results for the diagonal P-wave phase shifts of the $n + ^7$Li elastic scattering as well as the elastic ^{7}Li$(n,n)^7$Li and inelastic ^{7}Li$(n,n')^7$Li$(1/2^-)$ cross sections. At low energies, we can identify four resonances, two of which can be associated with the experimentally known ^{8}Li states: 3^+ at $E_x = 2.255$ MeV and 1^+ at $E_x = 3.21$ MeV [49]. The other two resonances, 0^+ and 2^+ are not present in the ^{8}Li evaluation of Ref. [49]. They do appear in many theoretical calculations, which include the GFMC [3], NCSM [48], and recoil-corrected continuum shell model (RCCSM) [51]. The 0^+ resonance also appears in the Generator Coordinate Method (GCM) calculations of Ref. [52]. Contributions of different resonances to the cross sections can be deduced from Fig. 9. The elastic cross section is dominated by the 3^+ resonance with some contributions from the 2^+ resonance at higher energy. The inelastic cross section shows a peak just above the threshold caused by the 0^+ resonance and also a contribution from the 1^+ resonance. The appearance of a 0^+ peak just above threshold of the ^{7}Li$(n,n')^7$Li$(1/2^-)$ reaction was also discussed in Ref. [51] (see Fig. 10 in that paper). The data of Ref. [50] seem to be inconclusive concerning a 0^+ state close to the threshold,

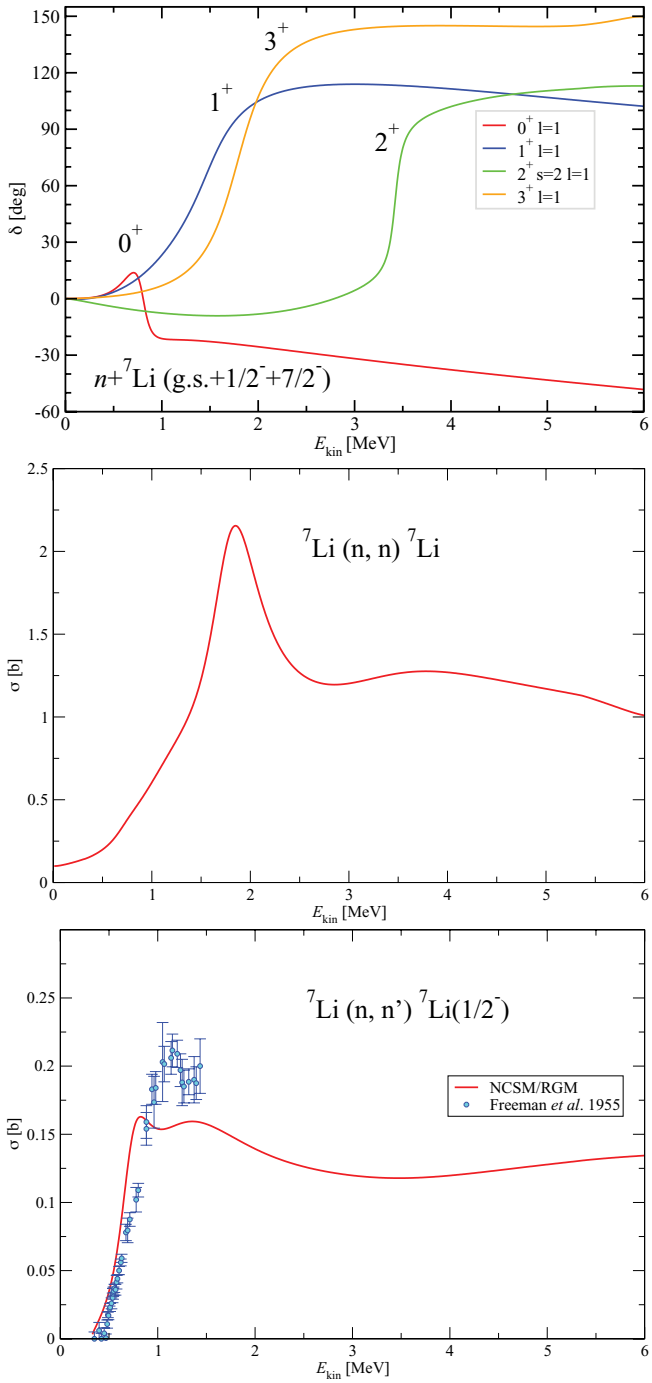

FIG. 9. (Color online) P-wave diagonal phase shifts of the n-^{7}Li elastic scattering (top panel), elastic ^{7}Li(n,n)^{7}Li cross section (middle panel), and inelastic ^{7}Li(n,n')^{7}Li(1/2$^-$) cross section (bottom panel). The NCSM/RGM calculations that included the ^{7}Li ground state and the 1/2$^-$ and 7/2$^-$ excited states were performed by using the SRG-N^{3}LO NN potential with $\Lambda = 2.02$ fm^{-1}. Wave functions from IT-NCSM calculations in the $N_{max} = 12$ basis and the HO frequency of $\hbar\Omega = 20$ MeV were employed. Experimental data are from Ref. [50].

see the bottom panel of Fig. 9. It is known, however, that the position of the 0^+ state is sensitive to the strength of the spin-orbit interaction [3,48,51]. The three-nucleon interaction, which would increase the strength of the spin-orbit force, was not included in our present calculations. Consequently, our predicted 0^+ state energy may be underestimated. We note that no fit to the experimental threshold was performed in the present NCSM/RGM calculations. Still, as seen in the bottom panel of Fig. 9, the calculated inelastic cross section is very close to the experimental data just above the threshold.

B. p-^{7}Be

In the mirror system p-^{7}Be, we do not find a bound state in the same type of coupled-channel NCSM/RGM calculation as described earlier for n-^{7}Li. As seen in the top and middle parts of Fig. 10, the lowest 2^+ resonance, which corresponds to the ^{8}B ground state lies at about 200 keV above the threshold. In the experiment, ^{8}B is bound by 137 keV [49]. Our calculated lowest 1^+ resonance appears at about 1 MeV. It corresponds to the experimental ^{8}B 1^+ state at $E_x = 0.77$ MeV (0.63 MeV above the p-^{7}Be threshold). This resonance dominates the inelastic cross section as seen in the bottom part of Fig. 10. The higher-lying resonances follow similar patterns as those found in n-^{7}Li (Fig. 9). Again, we find 0^+ and 2^+ resonances not included in the recent ^{8}B evaluation [49]. We note that experimental efforts are now under way to find these resonances [46,53]. In particular, the very recent Ref. [54] does claim observation of the low-lying 0^+ and 2^+ resonances based on the R-matrix analysis of the p-^{7}Be scattering experiment performed in the energy range between 1.6 and 2.8 MeV in the c.m. Their suggested 0^+ resonance at 1.9 MeV is quite close to our calculated 0^+ energy in the present paper. We further note that our calculated 1^+_2 states in ^{8}Li and ^{8}B appear at significantly higher energies than the corresponding 1^+_2 states obtained within the microscopic cluster model in Ref. [55].

The middle panel of Fig. 10 once again demonstrates the good accuracy of the IT calculations for a high $N\hbar\Omega$ $N_{max} = 10$ model space. The IT calculation reduced the ^{7}Be basis from 43.6 to 11.9 $\times$ 10^6 in the present case.

The elastic p-^{7}Be scattering was measured at 148° and was analyzed by the R-matrix approach [46]. Cross-sectional calculations within the RCCSM at that angle were then published in Ref. [56] and also in Ref. [51]. Furthermore, elastic and inelastic cross sections at this angle were analyzed within the time-dependent approach to the continuum shell model [57]. Our elastic and inelastic differential cross section results at 148° are presented in Fig. 11. In the elastic cross section, the first 1^+ state is visible and beyond the minimum of the cross section, we can see the dominant peak caused by the 3^+ state. At higher energies, the 2^+ state contributes as well. The inelastic cross section at 148° has a similar shape as the reaction cross section shown in Fig. 10. The first 1^+ state peak dominates at low energy with contributions from the 0^+ and the second 1^+ at higher energies. Our findings are in line with the RCCSM results. However, we remind the reader that there is no fitting in our calculations, all results are predictions based on the SRG-N^{3}LO NN potential. Because of this, the positions of our calculated resonances (e.g., 1^+, 3^+) do not exactly reproduce the experiment. We do not include the experimental data in the figure as they would be shifted compared to the calculated peaks. There are at least two reasons why our predictions do not match

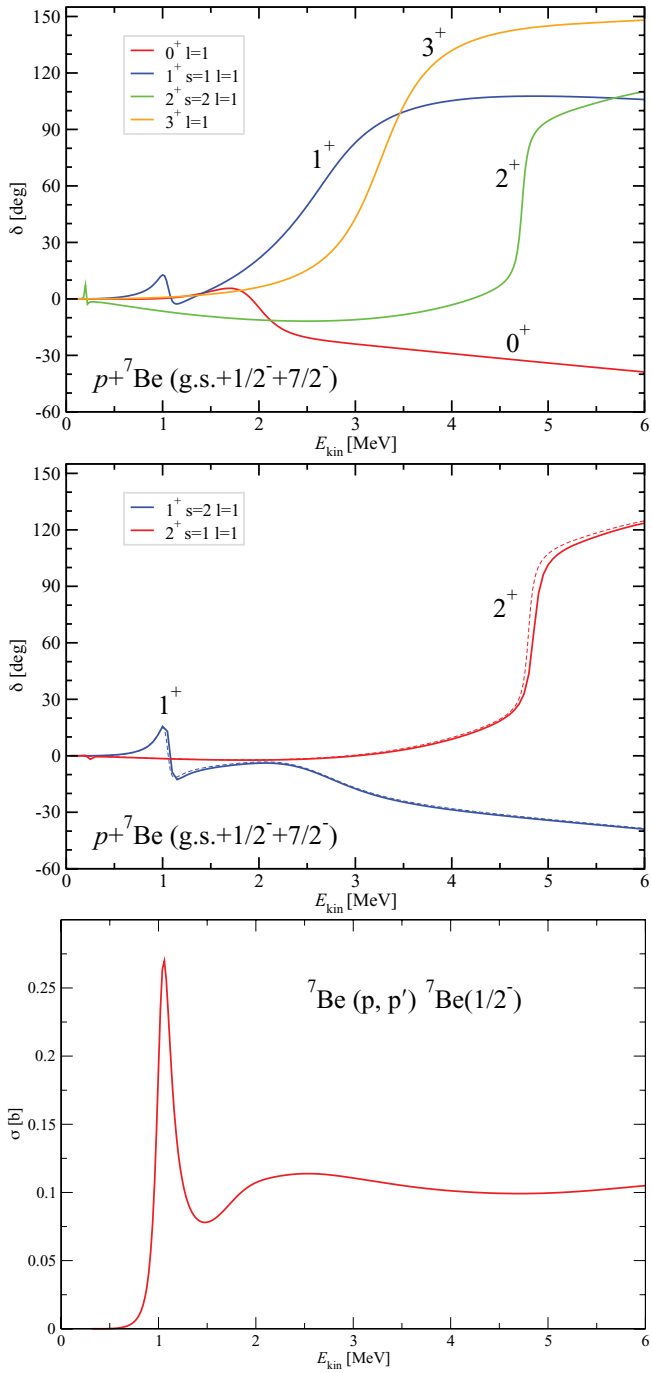

FIG. 10. (Color online) P-wave diagonal phase shifts of the p-^{7}Be elastic scattering (top and middle panels) and inelastic ^{7}Be(p, p')^{7}Be($1/2^-$) cross section (bottom panel). The NCSM/RGM calculations that included the ^{7}Be ground state and the $1/2^-$ and $7/2^-$ excited states were performed by using the SRG-N^{3}LO NN potential with $\Lambda = 2.02$ fm^{-1}. Wave functions from IT-NCSM calculations in the $N_{\max} = 12$ basis and the HO frequency of $\hbar\Omega = 20$ MeV were employed. In the middle panel, the full-space NCSM (solid lines) and the IT-NCSM (dashed lines) results in the $N_{\max} = 10$ basis are compared.

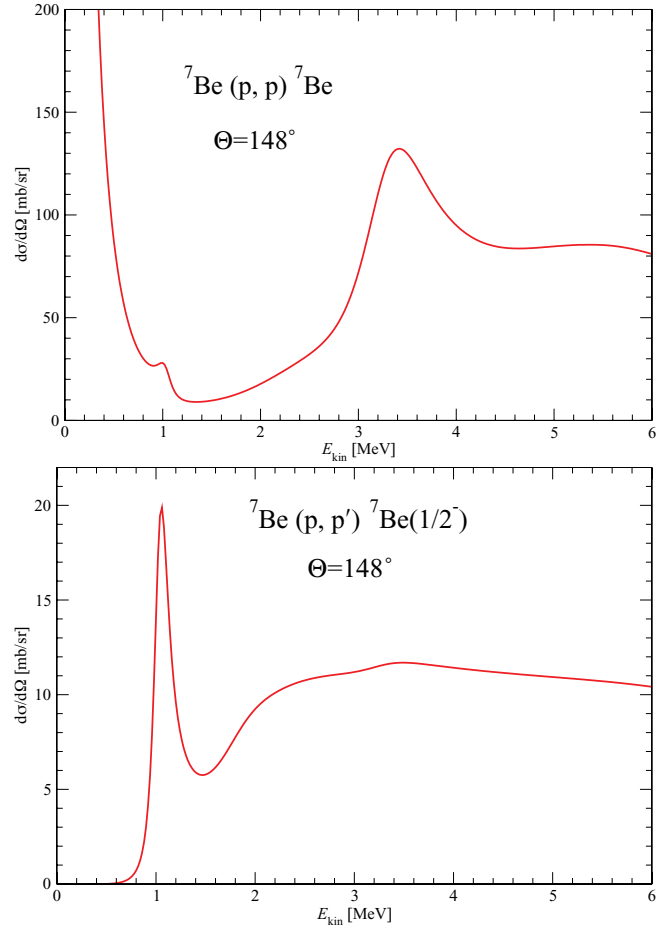

FIG. 11. (Color online) Elastic ^{7}Be(p, p)^{7}Be (top panel) and inelastic ^{7}Be(p, p')^{7}Be($1/2^-$) (bottom panel) differential cross sections at $\Theta_{\text{c.m.}} = 148^\circ$ calculated within the NCSM/RGM with the SRG-N^{3}LO NN potential with $\Lambda = 2.02$ fm^{-1}.

the experimental resonances accurately. First, our nuclear Hamiltonian is incomplete (e.g., no three-nucleon interaction is included). Second, we omitted higher resonances of ^{7}Li and ^{7}Be because of numerical reasons. Most likely, the omitted resonances would produce some shifts in the calculated peaks.

To address the issue of convergence of our results with the number of included excited states of ^{7}Be (or ^{7}Li), we performed smaller-space calculations with up to four excited states of ^{7}Be. It can be anticipated that the impact of excited states depends on the investigated energy range and the spin and parity of the partial wave. This is demonstrated in Fig. 12. In the top panel, we repeat our $N_{\max} = 12$ results for the 0^+ and 1^+ P waves from Fig. 10 compared to calculations with just the ground state and the ground state plus the lowest $1/2^-$ state. Clearly, the impact of the $7/2^-$ state is minimal. We confirmed in small-space $N_{\max} = 6$ calculations that the impact of the third and fourth excited states of ^{7}Be (and ^{7}Li), both of which are $5/2^-$ states, on these partial waves is minimal as well. It is a different situation for the 2^+ and the 3^+ partial waves as seen in the middle and bottom panels of Fig. 12. Even the 2^+ ground state is shifted to a lower energy by the $7/2^-$ state (close to zero in the presented $N_{\max} = 6$ calculation, invisible in the figure), and the ^{8}B becomes weakly bound once the $5/2^-$ states are included (this does not necessarily mean that the

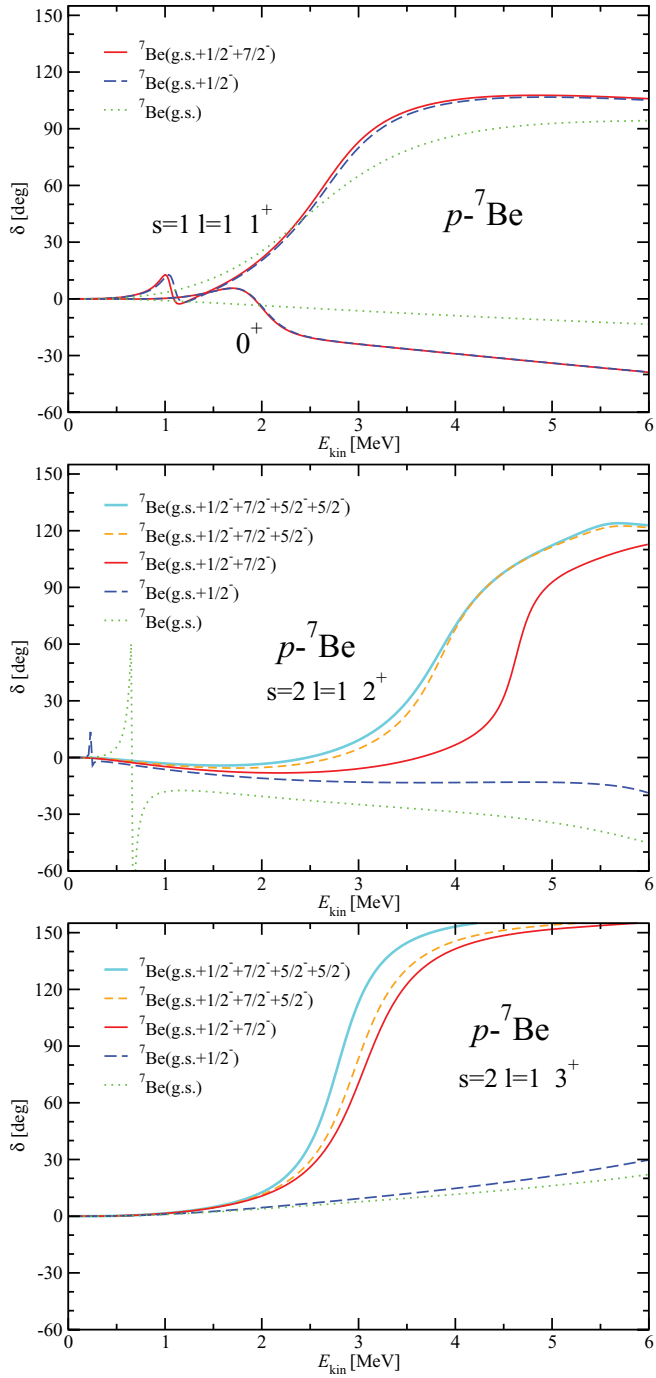

FIG. 12. (Color online) Dependence of the P-wave diagonal phase shifts of the p-^{7}Be elastic scattering on the number of included excited states of ^{7}Be. The $N_{\max} = 12$ basis (top panel) and $N_{\max} = 6$ basis (middle and bottom panels) were used with the SRG-N^{3}LO NN potential with $\Lambda = 2.02$ fm^{-1} and the HO frequency of $\hbar\Omega = 20$ MeV.

converged, or large-space $N_{\max} = 12$ calculation will produce a bound state with the $5/2^-$ states included). The 2^+ and 3^+ resonances do not appear until the $7/2^-$ state is included, and their position is shifted because of the $5/2^-$ states by about 1 MeV for the 2^+ and 0.5 MeV for the 3^+, respectively. After the shifts, their positions are much closer to their experimental

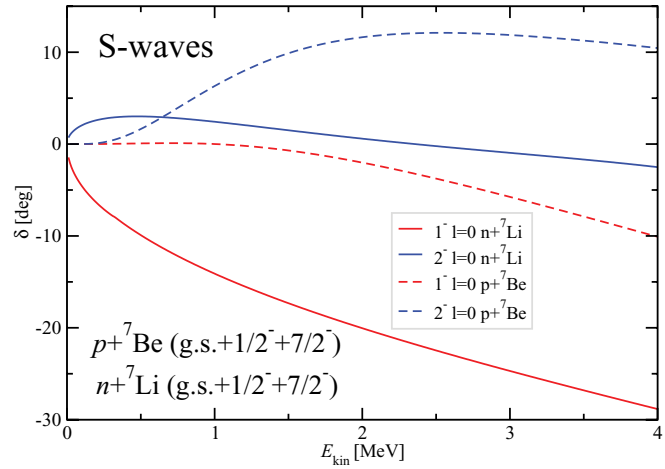

FIG. 13. (Color online) S-wave phase shifts of the $n + {}^7$Li (solid lines) and the $p + {}^7$Be (dashed lines) elastic scattering. The calculations as described in Figs. 9 and 10.

excitation energies of 2.28 MeV (3^+) and 2.55 MeV (2^+) from Ref. [54].

Both the inclusion of the three-nucleon interaction and the addition of more excited states of the target will be addressed in the future. The effect of higher excited states of ^{7}Be (^{7}Li) can be, in fact, most efficiently included by coupling the presently used NCSM/RGM basis with the ^{8}B (^{8}Li) NCSM eigenstates as outlined in Ref. [58]. Still, our current results contain the bulk of the physics behind the investigated scattering processes.

C. S-wave scattering lengths of n-^{7}Li and p-^{7}Be

In Fig. 13, we present our calculated n-^{7}Li and p-^{7}Be S-wave phase shifts. We do not find any evidence for a 2^- resonance advocated in Ref. [46] and discussed in Ref. [59]. The corresponding scattering lengths together with the experimental values are given in Table II. With the exception of the p-^{7}Be a_{01}, which has a large experimental uncertainty, our calculated scattering lengths do agree with experimental data as to their signs, however, there are differences in the absolute values. Again, as discussed before, the results presented here serve only as a first step toward the *ab initio* investigation of the n-^{7}Li and p-^{7}Be reactions. Prospects for a realistic calculation of the ^{7}Be$(p, \gamma)^8$B capture are excellent. Here, we found the ^{8}B unbound by only 200 keV. It is quite possible that ^{8}B will become bound (with the NN potential employed here: SRG-N^{3}LO with $\Lambda = 2.02$ fm^{-1}) by including more excited states of ^{7}Be in the coupled-channel NCSM/RGM

TABLE II. The n-^{7}Li and the p-^{7}Be S-wave scattering lengths. Theoretical values correspond to calculations as described in Figs. 9 and 10. Experimental values are from Refs. [45,47].

(fm)	^{7}Li		^{7}Be	
	Calc.	Expt.	Calc.	Expt.
a_{01}	+1.23	+0.87(7)	−1.2	25(9)
a_{02}	−0.61	−3.63(5)	−10.2	−7(3)

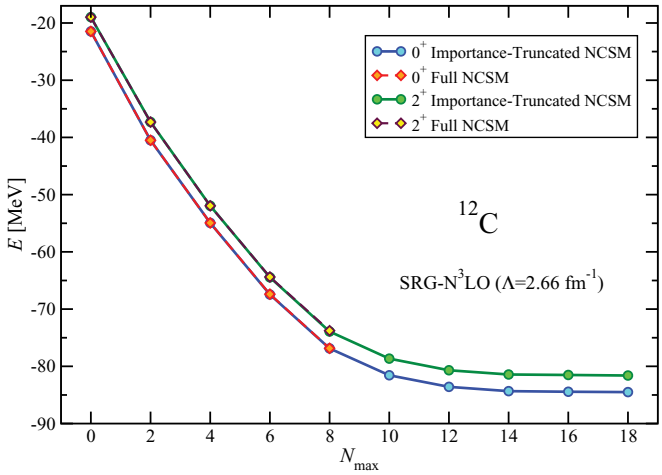

FIG. 14. (Color online) Ground-state and the first excited 2^+ state energy dependence on the model-space size $N_{\max}$ for ^{12}C, obtained within the IT-NCSM, by using the SRG-N^{3}LO NN potential with $\Lambda = 2.66$ fm^{-1}. The HO frequency $\hbar\Omega = 24$ MeV was employed. The calculation is variational. No NCSM effective interaction was used. The full NCSM results were obtained with the code ANTOINE [61].

calculations. See also the discussion at the end of Sec. IV B. Even if the ^{8}B would not be bound or, most likely, the threshold energy will not agree with the experiment, we have the possibility to explore a variation of the SRG NN potential evolution parameter Λ and to tune this parameter to fit the experimental threshold. We note that, for any Λ, the SRG-evolved NN potential will describe all two-nucleon properties as accurately as the original starting NN potential, here, the chiral N^{3}LO potential of Ref. [30]. It should be noted that, by adding the three-nucleon interaction, omitted in the present calculations because of computational reasons, the need for a fine-tuning should be significantly reduced (i.e., the results should become Λ independent).

V. NUCLEON-^{12}C SCATTERING

For nucleon scattering calculations on ^{12}C or heavier targets within the NCSM/RGM, the use of the IT becomes essential. For ^{12}C, the full-space NCSM calculations are currently limited to $N_{\max} = 8$ (although successful runs were already performed for $N_{\max} = 10$ on the biggest supercomputers with the latest version of the code MFD [60]). This is insufficient for reaching or approaching convergence of the ^{12}C NCSM calculations as seen from Fig. 14 and even more so for the NCSM/RGM scattering calculations. The IT calculations, on the other hand, are feasible up to $N_{\max} = 18$, where convergence is reached for both the ground state as well as the excited states. Our ^{12}C calculations are performed with the SRG-N^{3}LO NN potential with the evolution parameter $\Lambda = 2.66$ fm^{-1}, a higher value (i.e., shorter evolution, less soft) than that used for the lighter nuclei. The use of a small Λ results in large overbinding of heavier nuclei and a significant underestimation of their radii. As seen in Fig. 14, our converged ^{12}C binding energy is about 84.5(8) MeV,

TABLE III. Calculated ground-state energies of ^{3}H, ^{4}He, ^{12}C, and ^{16}O obtained by using the SRG-N^{3}LO NN potential with $\Lambda = 2.66$ fm^{-1} compared to experimental values.

$E_{\text{g.s.}}$ (MeV)	^{3}H	^{4}He	^{12}C	^{16}O
Calc.	−8.18	−27.26	−84.5(8)	−139.0(8)
Expt.	−8.48	−28.30	−92.16	−127.62]

smaller than the experimental value of 92 MeV and, further, the agreement of the full-space and IT results is perfect all the way up to $N_{\max} = 8$. Our calculated ground-state energies of ^{3}H, ^{4}He, ^{12}C, and ^{16}O obtained with the SRG-N^{3}LO NN potential with $\Lambda = 2.66$ fm^{-1} are summarized in Table III.

A. p-^{12}C

Our low-energy p-^{12}C phase-shift results are shown in Fig. 15. The comparison of the $N_{\max} = 16$ and $N_{\max} = 14$ results demonstrates good convergence with respect to the HO-basis expansion. The ^{12}C ground state and the first 2^+ state were included in the coupled-channels NCSM/RGM equations. We note that we also performed a phase-shift comparison of the full-space and the IT calculations up to $N_{\max} = 6$ and found a similarly perfect agreement as presented in Fig. 3 for n-^{4}He. In the present p-^{12}C calculations, we found a single bound state $1/2^-$ at -2.98 MeV, which corresponds to the ^{13}N ground state, bound experimentally by 1.94 MeV [62]. The lowest resonance in our calculation is $3/2^-$, barely visible at 0.25 MeV above threshold. In the experiment, this resonance is at 1.56 MeV. Our calculated $1/2^+$ resonance appears at about 1.5 MeV above threshold (in the experiment at 0.42 MeV above threshold) and the $5/2^+$ resonance at about 4.9 MeV (in the experiment at 2.61 MeV).

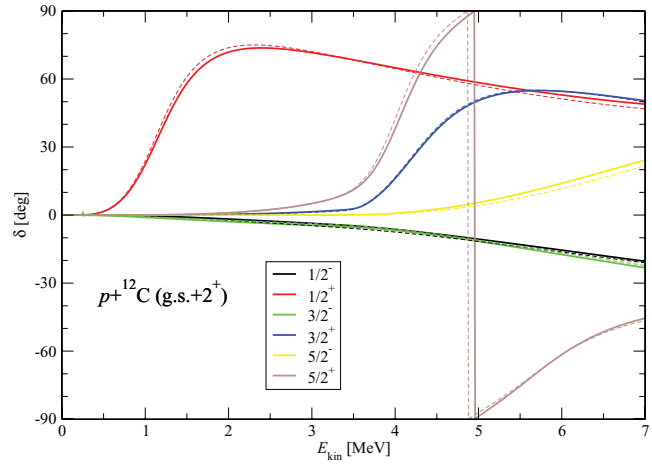

FIG. 15. (Color online) The p-^{12}C eigenphase shifts calculated within the NCSM/RGM by using the SRG-N^{3}LO NN potential with $\Lambda = 2.66$ fm^{-1} and the HO frequency $\hbar\Omega = 24$ MeV. Full lines (dotted lines) correspond to results obtained in the $N_{\max} = 16$ ($N_{\max} = 14$) model space. The ground state and the first excited 2^+ state of ^{12}C were included. The ^{12}C wave functions were obtained within the IT-NCSM.

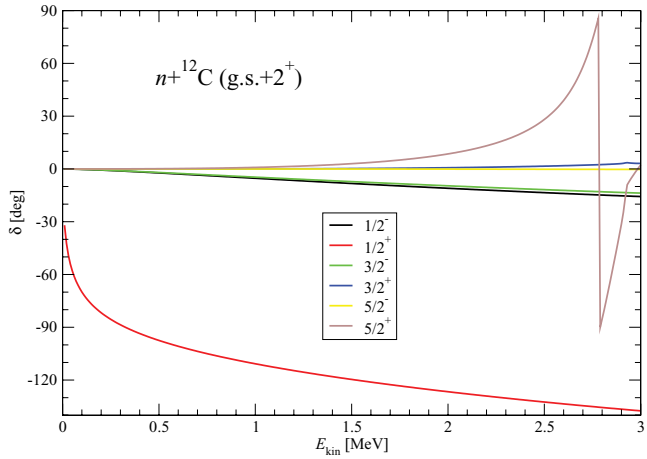

FIG. 16. (Color online) The n-^{12}C phase shifts calculated within the NCSM/RGM by using the SRG-N^{3}LO NN potential with $\Lambda = 2.66$ fm^{-1}. The HO frequency $\hbar\Omega = 24$ MeV and the model-spaces size of $N_{max} = 16$ were used. The ground state and the first excited 2^+ state of ^{12}C were included. The ^{12}C wave functions were obtained within the IT-NCSM.

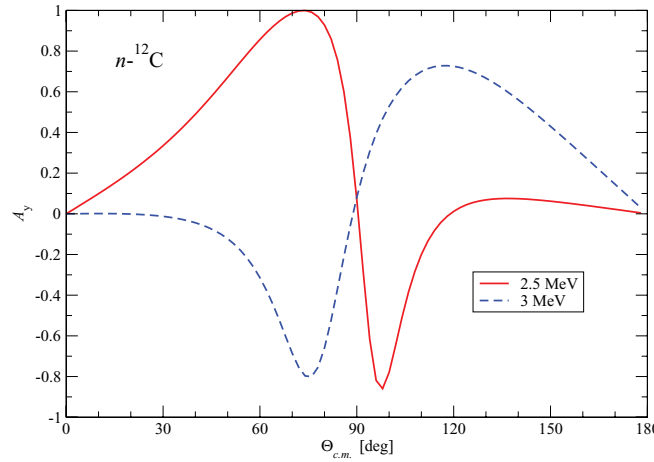

FIG. 17. (Color online) The analyzing power for n-^{12}C elastic scattering below and above the calculated $5/2^+$ resonance. Energies are in the c.m. The calculation as described in Fig. 16.

B. n-^{12}C

In the mirror system n-^{12}C, our NCSM/RGM calculations produce three bound states: $1/2^-$ at -5.34 MeV, which corresponds to the ^{13}C ground state experimentally bound by 4.95 MeV with respect to the n-^{12}C threshold, $3/2^-$ bound by 2.23 MeV (experimentally bound by 1.26 MeV), and $1/2^+$ bound by just 0.03 MeV (experimentally bound by 1.86 MeV). In the experiment, there is also a $5/2^+$ state bound by 1.09 MeV. Our present NCSM/RGM calculations, which include the lowest 0^+ and the lowest 2^+ ^{12}C states do not produce any bound $5/2^+$ state.

Our low-energy n-^{12}C diagonal phase shifts are shown in Fig. 16. The $5/2^+$ resonance is found at 2.8 MeV (experimentally at 1.92 MeV with respect to the n-^{12}C threshold). The steep drop of the $1/2^+$ phase shift is caused by the presence of the very weakly bound $1/2^+$ state. Similarly, we note that, as in the case of ^{11}Be, discussed in Ref. [18], we observe a significant decrease of the $1/2^+$ state energy in the n-^{12}C NCSM/RGM calculation when compared to the standard NCSM calculation for ^{13}C. We were able to make these comparisons in model spaces up to $N_{max} = 6$ where we found this drop to be about 3 MeV.

Analyzing powers were measured for proton and neutron scattering on ^{12}C [63–65], and scattering experiments on a polarized proton target are under way [66]. In Fig. 17, we present our calculated analyzing power below and above the energy of the $5/2^+$ resonance. We note that our calculated $5/2^+$ resonance appears at 2.8 MeV in the c.m. (experimentally at 1.92 MeV). Below the resonance, the analyzing power is positive at $\Theta_{c.m.} < 90^\circ$ and negative at $\Theta_{c.m.} > 90^\circ$. At energies above the resonance, the analyzing power reverses its sign. Similar observations were made in calculations performed within the multichannel algebraic scattering theory [67,68]. See, in particular, Fig. 5 of Ref. [68].

Our calculated ^{13}N and ^{13}C bound-state levels and resonances are more spread than the experimental ones. This is a consequence of an underestimation of the ^{12}C radius found to be 2.05 fm with the SRG-N^{3}LO NN potential. To remedy this, one would have to calculate three-nucleon interaction terms induced because of the SRG evolution. This can be performed as described in Ref. [69]. However, we still need to develop the NCSM/RGM formalism further to handle three-nucleon interactions in the scattering calculations.

VI. NUCLEON-^{16}O SCATTERING

The calculation of nucleon scattering on ^{16}O is the most challenging among the systems we investigate in this paper. The α clustering plays an important role in the structure of ^{16}O, in particular, for the first excited 0^+ state that is known to be almost impossible to reproduce in NCSM or coupled-cluster calculations. Our present calculations do not include the α clustering yet.

As in the case of ^{12}C, we rely on the IT-NCSM calculations for obtaining the ^{16}O wave functions as the full-N_{max} NCSM calculations are possible only up to $N_{max} = 8$. In Fig. 18, we show the ground-state convergence within the IT-NCSM and a comparison to the full-space results. Again, up to the largest accessible model space, the agreement between the IT and the full-space calculations is perfect.

A. n-^{16}O

It is straightforward to converge nucleon-^{16}O scattering calculations within the NCSM/RGM by using the HO expansion up to $N_{max} = 18$. Our calculated n-^{16}O phase shifts are shown in Fig. 19, and the HO-basis expansion convergence is checked for the S and D waves in Fig. 20. These calculations only included the ^{16}O ground state. We find two bound states, $1/2^+$ at -0.88 MeV and $5/2^+$ at -0.41 MeV with respect to the n-^{16}O threshold. In experiment, the ^{17}O ground state is $5/2^+$, bound by 4.14 MeV, and the $1/2^+$ state is the first excited state bound by 3.27 MeV. There are also two additional bound states: $1/2^-$ and $3/2^-$. Those are unbound in our calculations.

Clearly, it is insufficient to consider only the ground state of ^{16}O in the coupled-channel NCSM/RGM scattering

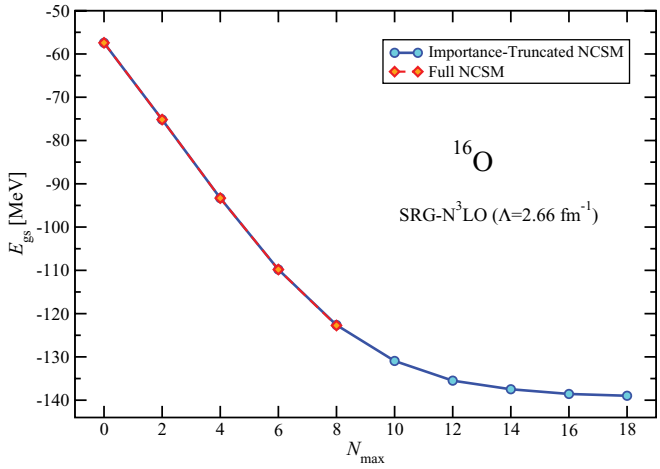

FIG. 18. (Color online) Ground-state energy dependence on the model-space size N_{max} for ^{16}O, obtained within the IT-NCSM by using the SRG-N^{3}LO NN potential with $\Lambda = 2.66$ fm^{-1}. The HO frequency $\hbar\Omega = 24$ MeV was employed. The calculation is variational. No NCSM effective interaction was used. The full NCSM results were obtained with the code ANTOINE [61].

calculations. Therefore, in addition, we include the three lowest ^{16}O negative-parity states: 3^-, 1^-, and 2^-. Because of computational limitations, in this case, we used HO-basis expansion up to N_{max}=13. By comparing Fig. 21 to Fig. 19, the 1p-1h negative-parity excited states of ^{16}O generate negative-parity resonances in ^{17}O. These resonances do appear, however, at much higher energy than in the experiment. The reason for this is the fact that our calculated ^{16}O 1p-1h states have excitation energy that is too large. In particular, our calculated 3^- excited state has an excitation energy of 15.99 MeV, while experimentally, it lies at just 6.13 MeV. One reason for the discrepancy is the softness of the SRG-N^{3}LO NN potential we use that results in an overall overbinding of the ^{16}O ground state and in an underestimation of its radius.

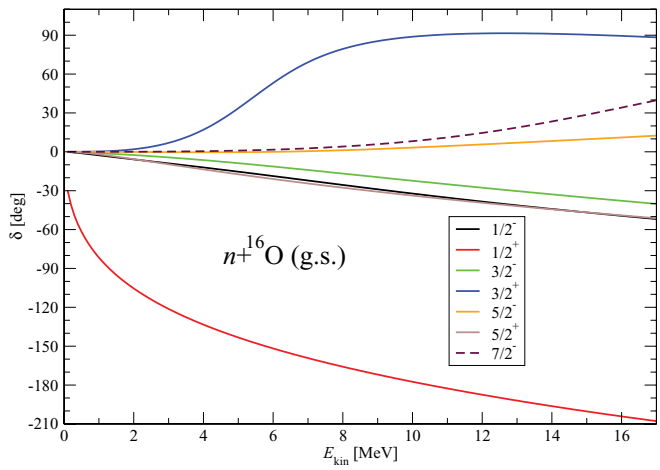

FIG. 19. (Color online) The n-^{16}O phase shifts calculated within the NCSM/RGM by using the SRG-N^{3}LO NN potential with $\Lambda = 2.66$ fm^{-1} and the HO frequency $\hbar\Omega = 24$ MeV in the $N_{max} = 18$ model space. The ground state of ^{16}O was included. The ^{16}O wave functions were obtained within the IT-NCSM.

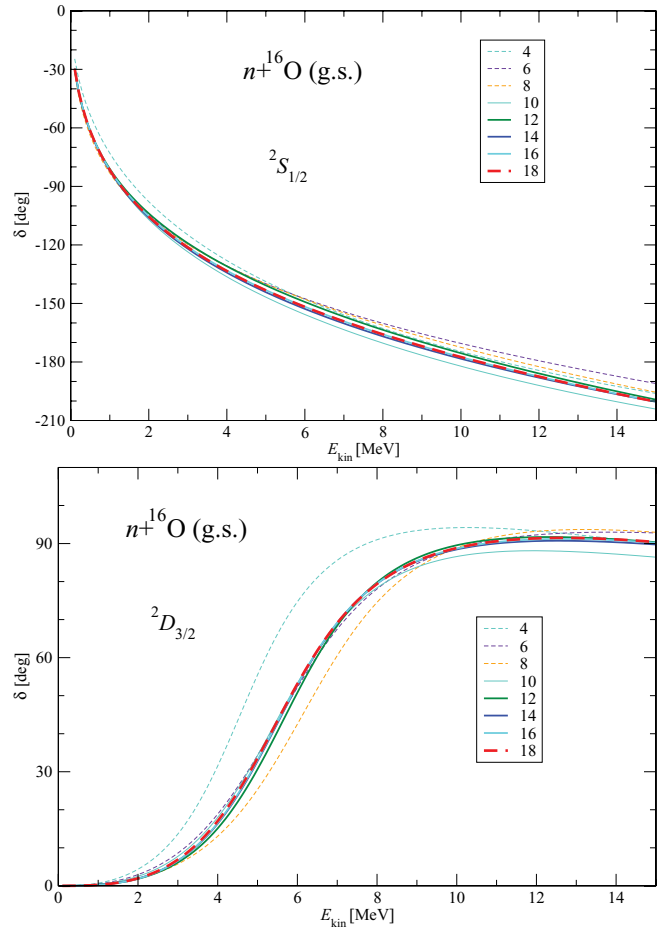

FIG. 20. (Color online) Basis size dependence of the n-^{16}O phase shifts calculated within the NCSM/RGM by using the SRG-N^{3}LO NN potential with $\Lambda = 2.66$ fm^{-1}. The HO frequency of $\hbar\Omega = 24$ MeV was used. The $J^\pi = 1/2^+(3/2^+)$ channel is shown in the top (bottom) panels. Model-space sizes up to $N_{max} = 18$ were considered. The ground state of ^{16}O was included. The ^{16}O wave functions were obtained within the IT-NCSM.

Another aspect is the challenging problem of the IT-NCSM extrapolations of the independent positive- and negative-parity state calculations. The uncertainties of the relative excitation energies are higher than in same-parity calculations. On the positive side, our calculation with the negative-parity states, although with overestimated excitation energies, results in the proper ordering of the ^{17}O bound states. The ground state is $5/2^+$ at -1.32 MeV, and the $1/2^+$ state gains binding as well, which appears at -1.03 MeV.

B. p-^{16}O

We also investigated the p-^{16}O scattering and ^{17}F states. When the NCSM/RGM calculations are restricted to the channels that only involve the ^{16}O ground state, we find a $1/2^+$ resonance at 1.0 MeV and a $5/2^+$ resonance at 2.2 MeV. These resonances correspond to the ^{17}F $1/2^+$ first excited state, bound by 0.105 MeV, and the ^{17}F $5/2^+$ ground state bound by 0.6 MeV with respect to the $p + ^{16}$O threshold. By coupling channels that involve the 1p-1h ^{16}O 3^-, 1^-, and 2^- excited states, the calculated $1/2^+$ and $5/2^+$ states are

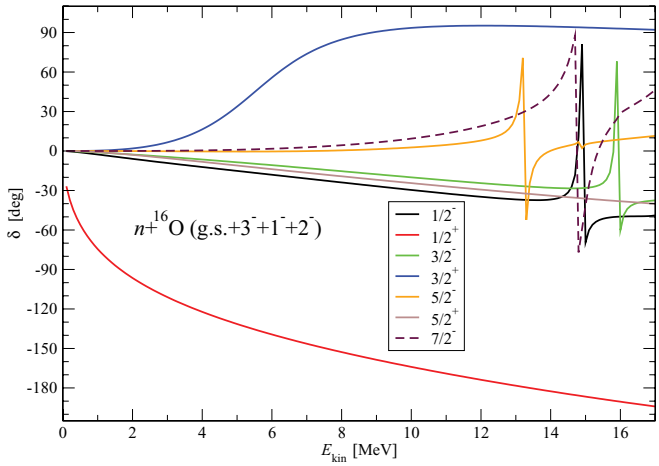

FIG. 21. (Color online) The n-^{16}O phase shifts calculated within the NCSM/RGM by using the SRG-N^{3}LO NN potential with $\Lambda = 2.66$ fm^{-1} and the HO frequency $\hbar\Omega = 24$ MeV in the $N_{\max} = 13$ model space. The ground state and the lowest 3^-, 1^-, and 2^- excited states of ^{16}O were included. The ^{16}O wave functions were obtained within the IT-NCSM.

still unbound resonances, but their energy moves significantly closer to the threshold: The $1/2^+$ appears at $+0.7$ MeV, and the $5/2^+$ appears at $+1.2$ MeV.

The ^{17}F low-lying states were recently investigated within the coupled-cluster approach with the Gamow-Hartree-Fock basis [70]. In those calculations with the N^{3}LO NN potential, the $1/2^+$ state is weakly bound, while the $5/2^+$ state remains unbound by about 0.1 MeV. By using the SRG-evolved interaction, the $5/2^+$ state became bound with the decrease of the SRG parameter Λ. We note that our calculated ^{16}O ground-state energy $-139.0(8)$ MeV (Fig. 18) obtained with the SRG-N^{3}LO NN potential with $\Lambda = 2.66$ fm^{-1}, compares well with the coupled-cluster singles-doubles ^{16}O calculations: -137.6 MeV with the SRG-N^{3}LO NN potential with $\Lambda = 2.8$ fm^{-1} [71]. The differences in the positions of the $1/2^+$ and $5/2^+$ are caused by deficiencies in our description of the negative parity 1p-1h states, which could be related to the two-body Hamiltonian used here as well as the uncertainties of the threshold extrapolations for the excitation energies. The inclusion of additional ^{16}O excited states would increase the absolute energy of our calculated ^{17}F states. The most efficient way to do this is by coupling the presently used NCSM/RGM basis with the ^{17}F NCSM eigenstates as outlined in Ref. [58].

VII. CONCLUSIONS

By combining the IT scheme for the cluster eigenstate basis with the *ab initio* NCSM/RGM approach, we were able to perform many-body calculations for nucleon scattering on nuclei with mass number as high as $A = 16$. With the soft SRG-evolved chiral NN potentials, convergence of the calculations with respect to the HO-basis expansion of the target eigenstates and the localized parts of the NCSM/RGM integration kernels can be reached by using $N_{\max} = 12$–16.

We first benchmarked the IT-NCSM results with the full-space NCSM results for the $A = 5$ system. Our neutron-^{4}He and proton-^{4}He calculations compare well with an R-matrix analysis of the data, in particular, at energies above 8 MeV, and describe well-measured cross sections and analyzing powers for those energies.

Our calculations of n-^{7}Li and p-^{7}Be scattering predict low-lying 0^+ and 2^+ resonances in ^{8}Li and ^{8}B that have not been experimentally clearly identified yet. We found that the prospects of a realistic *ab initio* calculation of the ^{7}Be$(p,\gamma)^8$B capture within our approach are very good. In the present calculations, we found the ^{8}B unbound by only 200 keV. It is quite possible that ^{8}B will become bound (with the NN potential employed here: SRG-N^{3}LO with $\Lambda = 2.02$ fm^{-1}) by including more excited states of ^{7}Be in the coupled-channel NCSM/RGM calculations. Even if the ^{8}B will still not be bound or, most likely, the threshold energy will not agree with the experiment, we have the possibility to explore a variation of the SRG NN potential evolution parameter Λ and to tune this parameter to fit the experimental threshold.

The use of the IT basis becomes essential in calculations with ^{12}C or ^{16}O targets as the full-space NCSM calculations are limited to $N_{\max} = 8$. Our n-^{12}C and p-^{12}C investigations included ^{12}C ground and the first excited 2^+ states. We found a single bound state $1/2^+$ in ^{13}N as in the experiment. In ^{13}C, we found three bound states with the $5/2^+$ state still unbound contrary to the experiment. Our calculated spectrum of $A = 13$ states is more spread than in the experiment because of the underestimation of the ^{12}C radius, a consequence of the softness of the SRG-evolved NN interaction.

The description of nucleon scattering on ^{16}O within our formalism was the most challenging. The α clustering that plays an important role in the structure of ^{16}O is not yet included in our present calculations. Furthermore, the 1p-1h ^{16}O excited states are more difficult to treat in the IT-NCSM approach, as the extrapolations of excitation energies are performed from the independent ground state and the negative-parity state calculations. We found a strong impact of the 1p-1h ^{16}O states on the positions of the lowest $A = 17$ states. For example, correct ordering of the $5/2^+$ and $1/2^+$ states in ^{17}O was obtained only when the 1p-1h states were included.

Overall, we find that the inclusion of additional excited states of the target nuclei would be beneficial in all studied systems and more significant with the increase of A. Coupled-channel NCSM/RGM calculations with many excited states of the target are computationally challenging. The most efficient way to include the effects of such states is by coupling the presently used NCSM/RGM basis, which consists of just a few lowest excited states, with the NCSM eigenstates of the composite system as outlined in Ref. [58]. Work on this coupling is under way.

The use of the SRG-evolved NN interaction facilitates convergence of the NCSM/RGM calculations with respect to the HO-basis expansion. On the other hand, because of the softness of these interactions, radii of heavier nuclei become underestimated. To remedy this, one would have to calculate three-nucleon interaction terms induced caused by the SRG evolution. This can be done as described in Ref. [69]. It is essential to further develop the NCSM/RGM formalism to handle three-nucleon interactions, both genuine and the SRG-evolution induced, in the scattering calculations.

In the present paper, we limited ourselves to single-nucleon projectile scattering. Extensions of the NCSM/RGM formalism to include deuteron, ^{3}H, and ^{3}He projectiles are under way.

ACKNOWLEDGMENTS

Numerical calculations have been performed at the LLNL LC facilities and at the NIC, Jülich. Prepared in part by LLNL under Contract No. DE-AC52-07NA27344. Support from the US DOE/SC/NP (Work Proposal No. SCW0498), LLNL LDRD Grant No. PLS-09-ERD-020, and from the US Department of Energy Grant No. DE-FC02-07ER41457 is acknowledged. This work is supported in part by the Deutsche Forschungsgemeinschaft through Contract No. SFB 634 and by the Helmholtz International Center for FAIR within the framework of the LOEWE program launched by the State of Hesse.

[1] H. Kamada *et al.*, Phys. Rev. C **64**, 044001 (2001).
[2] A. Nogga, H. Kamada, and W. Glöckle, Phys. Rev. Lett. **85**, 944 (2000).
[3] R. B. Wiringa, S. C. Pieper, J. Carlson, and V. R. Pandharipande, Phys. Rev. C **62**, 014001 (2000); S. C. Pieper and R. B. Wiringa, Annu. Rev. Nucl. Part. Sci. **51**, 53 (2001); S. C. Pieper, K. Varga, and R. B. Wiringa, Phys. Rev. C **66**, 044310 (2002).
[4] P. Navrátil and W. E. Ormand, Phys. Rev. C **68**, 034305 (2003).
[5] H. Witala, W. Glöckle, J. Golak, A. Nogga, H. Kamada, R. Skibinski, and J. Kuros-Zolnierczuk, Phys. Rev. C **63**, 024007 (2001).
[6] R. Lazauskas and J. Carbonell, Phys. Rev. C **70**, 044002 (2004).
[7] A. Kievsky, S. Rosati, M. Viviani, L. E. Marcucci, and L. Girlanda, J. Phys. G **35**, 063101 (2008).
[8] A. Deltuva and A. C. Fonseca, Phys. Rev. C **75**, 014005 (2007); Phys. Rev. Lett. **98**, 162502 (2007).
[9] K. M. Nollett, S. C. Pieper, R. B. Wiringa, J. Carlson, and G. M. Hale, Phys. Rev. Lett. **99**, 022502 (2007).
[10] G. Hagen, D. J. Dean, M. Hjorth-Jensen, and T. Papenbrock, Phys. Lett. B **656**, 169 (2007).
[11] P. Navrátil, J. P. Vary, and B. R. Barrett, Phys. Rev. Lett. **84**, 5728 (2000); Phys. Rev. C **62**, 054311 (2000).
[12] K. Wildermuth and Y. C. Tang, *A Unified Theory of the Nucleus* (Vieweg, Braunschweig, 1977).
[13] Y. C. Tang, M. LeMere, and D. R. Thompson, Phys. Rep. **47**, 167 (1978).
[14] T. Fliessbach and H. Walliser, Nucl. Phys. A **377**, 84 (1982).
[15] K. Langanke and H. Friedrich, *Advances in Nuclear Physics*, edited by J. W. Negele and E. Vogt (Plenum, New York, 1986).
[16] R. G. Lovas, R. J. Liotta, A. Insolia, K. Varga, and D. S. Delion, Phys. Rep. **294**, 265 (1998).
[17] H. M. Hofmann and G. M. Hale, Phys. Rev. C **77**, 044002 (2008).
[18] S. Quaglioni and P. Navrátil, Phys. Rev. Lett. **101**, 092501 (2008).
[19] S. Quaglioni and P. Navrátil, Phys. Rev. C **79**, 044606 (2009).
[20] P. Descouvemont, C. Daniel, and D. Baye, Phys. Rev. C **67**, 044309 (2003).
[21] P. Descouvemont, E. Tursunov, and D. Baye, Nucl. Phys. A **765**, 370 (2006).
[22] M. Theeten, D. Baye, and P. Descouvemont, Phys. Rev. C **74**, 044304 (2006).
[23] M. Theeten, H. Matsumura, M. Orabi, D. Baye, P. Descouvemont, Y. Fujiwara, and Y. Suzuki, Phys. Rev. C **76**, 054003 (2007).
[24] D. Baye, P. Capel, P. Descouvemont, and Y. Suzuki, Phys. Rev. C **79**, 024607 (2009).
[25] R. Roth and P. Navrátil, Phys. Rev. Lett. **99**, 092501 (2007).
[26] R. Roth, Phys. Rev. C **79**, 064324 (2009).
[27] S. K. Bogner, R. J. Furnstahl, and R. J. Perry, Phys. Rev. C **75**, 061001 (2007).
[28] R. Roth, S. Reinhardt, and H. Hergert, Phys. Rev. C **77**, 064003 (2008).
[29] R. Roth, T. Neff, and H. Feldmeier, Prog. Part. Nucl. Phys. **65**, 50 (2010).
[30] D. R. Entem and R. Machleidt, Phys. Rev. C **68**, 041001(R) (2003).
[31] R. Roth, J. R. Gour, and P. Piecuch, Phys. Rev. C **79**, 054325 (2009).
[32] R. Roth, J. R. Gour, and P. Piecuch, Phys. Lett. B **682**, 27 (2009).
[33] S. K. Bogner, T. T. S. Kuo, and A. Schwenk, Phys. Rep. **386**, 1 (2003); G. Hagen (private communication).
[34] R. Machleidt, Phys. Rev. C **63**, 024001 (2001).
[35] G. M. Hale (private communication).
[36] H. Krupp, J. C. Hiebert, H. O. Klages, P. Doll, J. Hansmeyer, P. Plischke, J. Wilczynski, and H. Zankel, Phys. Rev. C **30**, 1810 (1984).
[37] P. Schwandt, T. B. Clegg, and W. Haeberli, Nucl. Phys. A **163**, 432 (1971).
[38] K. W. Brokman, Phys. Rev. **108**, 1000 (1957).
[39] D. C. Dodder, G. M. Hale, N. Jarmie, J. H. Jett, P. W. Keaton Jr., R. A. Nisley, and K. Witte, Phys. Rev. C **15**, 518 (1977).
[40] R. A. Hardekopf and G. G. Holsen, Phys. Rev. C **15**, 514 (1977).
[41] E. Adelberger *et al.*, Rev. Mod. Phys. **70**, 1265 (1998).
[42] S. N. Ahmed *et al.* (SNO Collaboration), Phys. Rev. Lett. **92**, 181301 (2004).
[43] S. Couvidat, S. Turck-Chièze, and A. G. Kosovichev, Astrophys. J. **599**, 1434 (2003).
[44] J. N. Bahcall and M. H. Pinsonneault, Phys. Rev. Lett. **92**, 121301 (2004).
[45] C. Angulo *et al.*, Nucl. Phys. A **716**, 211 (2003).
[46] G. V. Rogachev *et al.*, Phys. Rev. C **64**, 061601(R) (2001).
[47] L. Koester, K. Knopf, and W. Waschkowski, Z. Phys. A **312**, 81 (1983).
[48] P. Navratil, C. A. Bertulani, and E. Caurier, Phys. Lett. B **634**, 191 (2006); Phys. Rev. C **73**, 065801 (2006).
[49] D. R. Tilley *et al.*, Nucl. Phys. A **745**, 155 (2004).
[50] J. M. Freeman, A. M. Lane, and B. Rose, Philos. Mag. **46**, 17 (1955).
[51] D. Halderson, Phys. Rev. C **73**, 024612 (2006).
[52] P. Descouvemont and D. Baye, Nucl. Phys. A **567**, 341 (1994).
[53] U. Greife *et al.*, Nucl. Instrum. Methods B **261**, 1089 (2007).
[54] J. P. Mitchell, G. V. Rogachev, E. D. Johnson, L. T. Baby, K. W. Kemper, A. M. Moro, P. N. Peplowski, A. Volya, and I. Wiedenhöver, Phys. Rev. C **82**, 011601(R) (2010).
[55] A. Csoto, Phys. Rev. C **61**, 024311 (2000).
[56] D. Halderson, Phys. Rev. C **69**, 014609 (2004).
[57] A. Volya, Phys. Rev. C **79**, 044308 (2009).

[58] P. Navratil, S. Quaglioni, I. Stetcu, and B. R. Barrett, J. Phys. G **36**, 083101 (2009).
[59] F. C. Barker and A. M. Mukhamedzhanov, Nucl. Phys. A **673**, 526 (2000).
[60] J. P. Vary (unpublished).
[61] E. Caurier, G. Martinez-Pinedo, F. Nowacki, A. Poves, J. Retamosa, and A. P. Zuker, Phys. Rev. C **59**, 2033 (1999); E. Caurier and F. Nowacki, Acta Phys. Pol. B **30**, 705 (1999).
[62] F. Ajzenberg-Selove, Nucl. Phys. A **523**, 1 (1991).
[63] W. Trachslin and L. Brown, Nucl. Phys. A **101**, 273 (1967).
[64] C.-C. Hsu, Y.-C. Yang, and T.-J. Lee, Chin. J. Phys. (Taipei) **4**, 49 (1966).
[65] C. D. Roper *et al.*, Phys. Rev. C **72**, 024605 (2005).
[66] A. Galindo Uribarri (private communication).
[67] G. Pisent, J. P. Svenne, L. Canton, K. Amos, S. Karataglidis, and D. van der Knijff, Phys. Rev. C **72**, 014601 (2005).
[68] J. P. Svenne, K. Amos, S. Karataglidis, D. van der Knijff, L. Canton, and G. Pisent, Phys. Rev. C **73**, 027601 (2006).
[69] E. D. Jurgenson, P. Navratil, and R. J. Furnstahl, Phys. Rev. Lett. **103**, 082501 (2009).
[70] G. Hagen, T. Papenbrock, and M. Hjorth-Jensen, Phys. Rev. Lett. **104**, 182501 (2010).
[71] T. Papenbrock (private communication).